A decade of summertime measurements of phytoplankton biomass, productivity and assemblage composition in the Pacific Arctic Region from 2006 to 2016

K.E. Giesbrecht[a,*], D.E. Varela[a,b,**], J. Wiktor[c], J.M. Grebmeier[d], B. Kelly[b], J.E. Long[b]

[a] School of Earth and Ocean Sciences, University of Victoria, Victoria, Canada
[b] Department of Biology, University of Victoria, Victoria, Canada
[c] Department of Marine Ecology, Institute of Oceanology of the Polish Academy of Sciences, Sopot, Poland
[d] Chesapeake Biological Laboratory, University of Maryland Center for Environmental Science, Solomons, MD 20688, USA

ARTICLE INFO

ABSTRACT

We present phytoplankton and nutrient observations from a period of ten years within five biological 'hotspots' in the Bering and Chukchi Seas, as identified by the Distributed Biological Observatory (DBO). Nitrate (NO_3^-) and total and size-fractionated ($<$ and $>$ 5 µm) chlorophyll *a* (Chl *a*) concentrations, and rates of carbon (ρC, 'primary productivity') and NO_3^- utilization (ρNO_3) were measured throughout the euphotic zone during eight cruises in July 2006, 2008 and yearly from 2011 to 2016. Samples were collected at one station within each of these five hotspots, which were located south of St. Lawrence Island (DBO1), south of the Bering Strait in the Chirikov Basin (DBO2), in the southeastern (DBO3) and northeastern (DBO4) Chukchi Sea, and in Barrow Canyon (DBO5). Nitrate concentrations averaged over the 10 years increased with depth and euphotic-zone integrated values were highest in the Chirikov Basin. Subsurface maxima in Chl *a* were present at about 30 m depth at most locations during every cruise, although the maximum ρC and ρNO_3 rates were shallower, within the top 10 m of the water column. The *f*-ratio (calculated as $\rho NO_3/\rho$C) averaged for all DBO regions and for the 10-year study-period was 0.41 ($\pm$ 0.24). Similarly, phytoplankton $>$ 5 µm in size accounted for 65 ($\pm$ 23) % of total Chl *a* for all regions over the 10 years. Taxonomic analysis done in 2013 showed that diatoms were the dominant taxa throughout all of the DBO regions, with the exception of areas influenced by low-nutrient waters on the eastern side of the Chukchi shelf near the Alaska coast. These coastal waters were dominated by coccolithophores and small ($<$ 7 µm) flagellates and had much lower Chl *a* concentrations, ρC and ρNO_3 than farther west. In addition, the proportion of pennate diatoms to total diatom abundance was found to be elevated relative to centric diatoms when sea-ice was present. Our measurements of phytoplankton biomass and ρC indicated that the higher abundance of pennate diatoms in the euphotic zone was the result of phytoplankton blooms happening below the ice, rather than pennate diatoms being supplied by a sea-ice diatom bloom. The dynamic nature of the Pacific Arctic Region (PAR) resulted in strong interannual variability within each DBO region for all parameters, with no clear increasing or decreasing trends from 2006 to 2016. Spatial variations were more consistent, with the highest rates of ρC and ρNO_3 occurring in the nutrient-rich waters of the southeastern Chukchi Sea (away from shore), and decreasing in regions further north as NO_3^- concentrations were lower. An east-west gradient in phytoplankton biomass and productivity was also observed in the southeastern Chukchi Sea, which can be attributed to differences in the nutrient content of the water masses along the gradient. This study shows that the observed strong interannual variability in phytoplankton biomass and productivity cannot be attributed to differences in methodology or sampling time. It also highlights the need for better temporal and spatial sampling resolution such that the long-term effects of climate-induced changes can be identified against the backdrop of the naturally-strong interannual variability in the PAR.

* Corresponding author.
** Corresponding author at: School of Earth and Ocean Sciences, University of Victoria, Victoria, Canada.
 E-mail addresses: karinag@uvic.ca (K.E. Giesbrecht), dvarela@uvic.ca (D.E. Varela).

1. Introduction

The Pacific Arctic Region (PAR) extends from the northern Bering Sea, through the Chukchi Sea, and into the western Beaufort Sea, and contains some of the most productive waters in the world's oceans (Springer and McRoy, 1993). Biological and physical processes in this region are strongly influenced by the northward advection of Pacific waters that supply nutrients, heat and freshwater to the PAR and subsequently to the Arctic Ocean (Grebmeier et al., 2006a; Serreze et al., 2006; Woodgate et al., 2010). In addition, climate-induced changes such as declining seasonal sea-ice extent and earlier sea-ice retreat (e.g. Frey et al., 2014, 2015; Stroeve et al., 2014) are affecting the biological state in this region, driving rapid shifts in ecosystem structure and function (e.g. Grebmeier, 2012; Nelson et al., 2014).

The flow of Pacific waters from the northern Bering Sea into the Chukchi Sea is primarily driven by a sea-level gradient towards the Chukchi Sea (Coachman and Aagaard, 1966; Stigebrandt, 1984; Woodgate et al., 2005a), with seasonal variability in the strength of the transport as a result of wind-driven forcing. Prevailing winds in this region are opposite to the pressure-driven flow such that the mean northward transport through the Bering Strait is at a maximum in the summer when winds are weaker, and at a minimum in the winter when winds are stronger (Woodgate, 2018; Woodgate et al., 2005b; Danielson et al., 2014). Waters flowing from the northern Bering Sea into the Bering Strait are made up of three major water masses (Fig. 1a) differentiated primarily by their temperature, salinity and nutrient characteristics: cold, saline, and nutrient-rich Anadyr Water (AW) on the western side; warm, less saline, and nutrient-poor Alaskan Coastal Water (ACW) on the eastern side; and Bering Shelf Water of intermediate characteriscs in the middle (Coachman et al., 1975; Walsh et al., 1989). As these waters flow through the Bering Strait, Bering Shelf Water and AW merge into a water mass known as Bering Sea Water (BSW). The southwestern region of the Chukchi Sea is also influenced by nutrient-poor waters from the south-flowing Siberian Coastal Current (SCC), although their contribution to the overall water mass mixture in the Chukchi Sea is small (Weingartner et al., 1999). More than ~80% of the water flowing into the Chukchi Sea through the Bering Strait is composed of nutrient-rich BSW (Coachman et al., 1975), which, in combination with the shallow bathymetry of the Chukchi shelf, support the high productivity observed in the Chukchi region.

Quantifying the autotrophic drawdown of nutrients, primary productivity and export of organic matter in the PAR is crucial for understanding the status and health of the local marine ecosystems and of other areas of the Arctic influenced by these waters (Carmack and Wassmann, 2006; Yamamoto-Kawai et al., 2006). Measurements of phytoplankton biomass (as chlorophyll *a*, Chl *a*) and pelagic primary productivity (as utilization rates of ^{13}C or ^{14}C) are standard methods used to assess the biological state of autotrophic organisms in marine environments. However, a broader picture of the ecology of the region can be provided by additional measurements of NO_3^- utilization rates using ^{15}N-labeled NO_3^-, used as an index of new production into a system, and by the assessment of the taxonomic composition of the phytoplankton assemblages. New production is defined as the autotrophic utilization rate of 'new' N sources (primarily NO_3^-) to the euphotic zone, which, on an annual basis and at steady state, can be considered equivalent to net community production, or the total amount of C available for export. Measurements of NO_3^- and C utilization rates can also be used to estimate the *f*-ratio, an index of the proportion of total primary production available for export (Eppley and Peterson, 1979). In addition to evaluating the status of autotrophic organisms, these measurements are powerful tools for assessing the cascading effects that changes at the bottom of marine food webs might have on higher trophic levels.

The high productivity on the continental shelves of the northern Bering and Chukchi Seas (e.g. Sakshaug et al., 2004; Varela et al., 2013) supports a diverse ecosystem with strong benthic-pelagic coupling (e.g.

Grebmeier and McRoy, 1989; Grebmeier et al., 2006a). Measurements of daily C utilization rates on these shelves include some of the highest values ever documented in the ocean (12 g C m^{-2} d^{-1} from McRoy et al., 1987), and annual estimates range from 100 to 720 g C m^{-2} yr^{-1} (Sakshaug et al., 2004; Brown et al., 2011; Varela et al., 2013; Hill et al., 2017). Nitrate utilization rates and phytoplankton biomass in these regions are twice as high as in the Beaufort Sea and Canadian Arctic Archipelago (Varela et al., 2013), and phytoplankton assemblages are generally dominated by diatoms (e.g. Wyatt et al., 2013; Crawford et al., 2018). Shallow water-columns and low zooplankton grazing pressures (e.g. Campbell et al., 2009; Sherr et al., 2009, 2013; Mathis et al., 2014) tightly couple pelagic primary production to the benthos (Grebmeier et al., 2006a), with these productive waters sustaining some of the highest benthic faunal biomass in the world's oceans (Grebmeier and McRoy, 1989; Highsmith and Coyle, 1990; Grebmeier et al., 2015). As a result, the PAR is both ecologically and economically important, supporting large and diverse populations of fishes, seabirds and marine mammals (e.g. Grebmeier et al., 2006a). It is also one of the fastest changing marine environments, with significant shifts in upper trophic levels in recent decades (e.g. Overland and Stabeno, 2004; Moore et al., 2014; Moore, 2016; Divoky et al., 2015).

Due to dramatic climate-induced environmental changes in the PAR (e.g. Stabeno et al., 2007; Woodgate et al., 2012; Jeffries et al., 2013; Wood et al., 2015), there is growing consensus that the Arctic is changing at a rate faster than any marine ecosystem can naturally adapt (Wassmann et al., 2010), and it is therefore reaching a 'tipping' point (Duarte et al., 2012). Some of the most significant changes in the PAR are decreasing sea-ice extent, earlier melting of the seasonal ice pack, and a shift from multi-year ice to thinner, first-year ice (e.g. Jeffries et al., 2013; Stroeve et al., 2014; Frey et al., 2014, 2015); however, these changes are not uniform across the PAR. The Chukchi Sea has experienced some of the fastest declines in sea-ice cover in the Arctic due to significant year-round warming (e.g. Cavalieri and Parkinson, 2012), whereas changes in the northern Bering Sea have resulted in more complex, multi-year variability in sea-ice cover (Frey et al., 2015). Regardless, these changes can have a major impact on both the timing and magnitude of primary productivity with potential cascading effects on higher trophic levels. However, due to the naturally-high spatial, seasonal, and interannual variability in the PAR, the extent to which these changes can be attributed to bottom-up pressures of climate change is still unclear (Grebmeier et al., 2010).

The Distributed Biological Observatory (DBO) (http://pmel.noaa.gov/dbo) was established in 2010 to assess the effects of climate change on the physical and biological state of the PAR (Grebmeier et al., 2010; Moore and Grebmeier, 2018). Sampling for the DBO occurs along a series of five transects that are centered on 'biological hotspots', identified by previous studies as locations of elevated productivity, biodiversity and rates of biological change (Fig. 1b). These five hotspots are located within the influence of the St. Lawrence Island Polynya (DBO1), in the Chirikov Basin between St. Lawrence Island and the Bering Strait (DBO2), in the southeastern (DBO3) and northeastern (DBO4) Chukchi Sea, and in Barrow Canyon (DBO5). Transects have been re-occupied both seasonally and annually by a number of participating international collaborators under the umbrella of DBO since 2010 and other programs prior to 2010 to help elucidate seasonal and interannual variability in the PAR.

Here, we present measurements of NO_3^- concentrations, and phytoplankton biomass, productivity and assemblage composition collected using consistent methodologies within the five DBO regions that span the period from 2006 to 2016. The main objectives of this study were to: (1) quantify a baseline of these measurements for current and future studies, (2) investigate the extent of the spatial and interannual variability between and, whenever possible, within each DBO region, and (3) elucidate potential environmental controls on this variability to better predict how phytoplankton dynamics might vary under current and predicted climate changes.
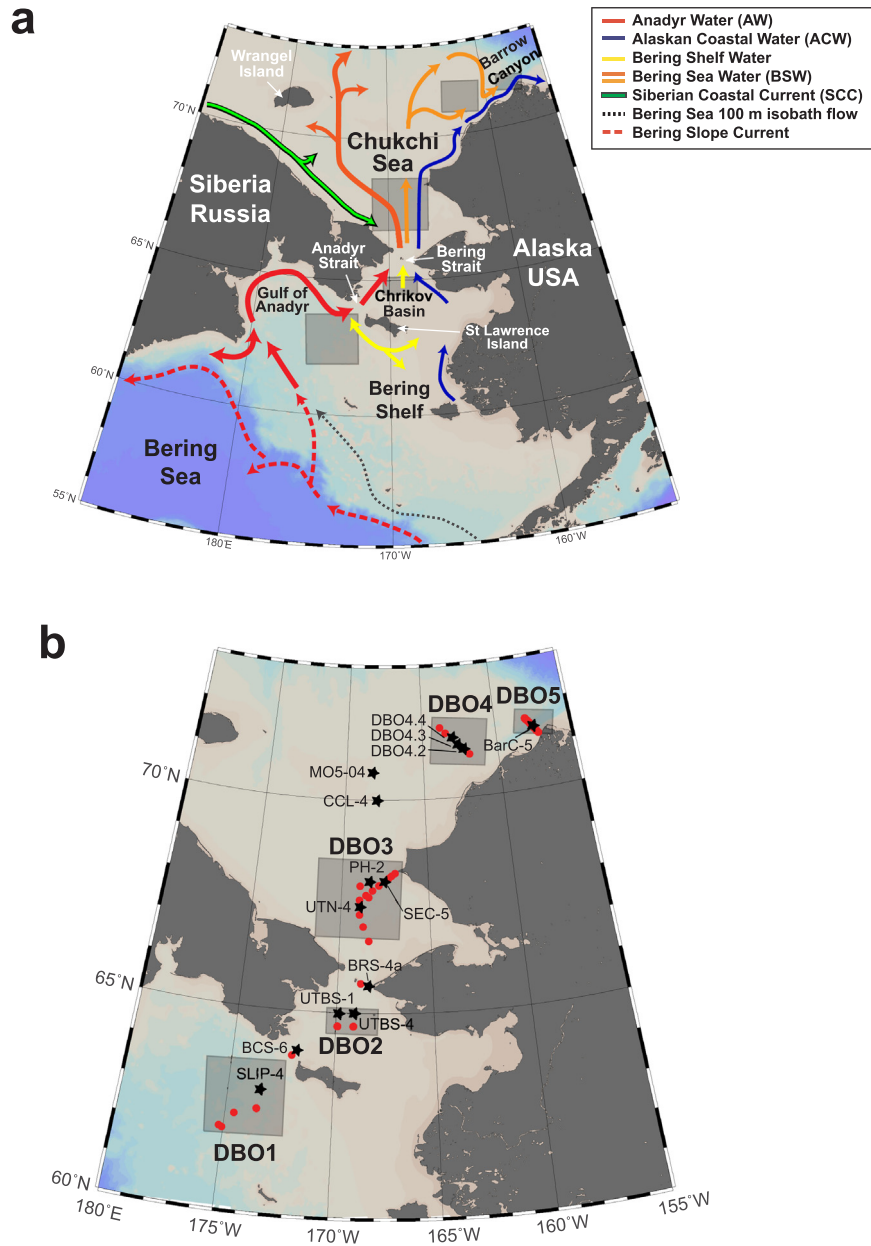
Fig. 1. (a) Map of the Pacific Arctic Region (PAR) with major geographical features, water mass flow patterns, and DBO region bounding boxes in grey. (b) DBO CTD/rosette station locations (red circles) and bounding boxes for each DBO region. Stations where phytoplankton productivity experiments were conducted are marked with a black star.
Adapted from Grebmeier et al. (2015) with updated flow patterns for the Bering Slope Current and Bering Sea 100 m isobath flow from Stabeno et al. (2016).

2. Methods

2.1. Sampling locations

Seawater samples were collected on eight oceanographic cruises onboard the *CCGS Sir Wilfrid Laurier* in July of 2006, 2008 and yearly from 2011 to 2016. Data from stations occupied in 2006 and 2008 are included when these stations were located within (or near) the identified DBO hotspot regions. The cruise conducted in 2006 was part of the Bering Strait Environmental Observatory program, while the cruise in 2008 was part of the International Polar Year Canada's Three Oceans (IPY-C3O) program. The 2008 data presented here represents a subset of the data already published in Varela et al. (2013) (nutrients and productivity) and Wyatt et al. (2013) (size fractionated Chl *a*). We include the 2008 data in this paper to provide a historical context to our

data from 2006 and to our DBO dataset from 2011 onwards. A maximum of 54 CTD/rosette stations distributed along 5 transects were occupied on each cruise for water column and sediment studies (red circles in Fig. 1b; Table 1), but primary productivity experiments were only conducted at 1–2 'primary productivity' stations per transect per year (black stars in Fig. 1b; Table 2). The aim was to conduct primary productivity experiments at the same stations within each region every year, although this was not always logistically possible due to ice and weather conditions. In particular, sampling in the eastern sector of DBO3 and in DBO5 occurred on only two out of the eight cruises (Table 2). Data from stations in DBO3 are separated into 'eastern' (DBOE, station SEC-5) and 'western' (DBO3W, stations UTN-4 and PH-2) sectors due to the significant spatial differences in water mass properties across this region.

Table 1

Summary of the number of CTD/rosette stations, productivity stations and DBO regions sampled on each of the six DBO cruises from 2011 to 2016 and from previous cruises not affiliated with DBO but in the same area (2006 & 2008).

Cruise ID[a] (YEAR-ID)	Cruise Dates	Total number of CTD/rosette stations	Total number of Productivity stations	DBO regions[b]	CTD/rosette data reference
2006–01[c]	Jul 1–29	19	4	*1, 2, 3, 4*	Cooper and Grebmeier (2016a)
2008–02[d]	Jul 3–27	16	5	*1, 2, 3, 4, 5*	Cooper and Grebmeier (2016b)
2011–18	Jul 6–21	37	3	*1, 2, 3, 5*	Cooper et al. (2016a)
2012–09	Jul 4–22	26	3	*1, 2, 3*	Cooper et al. (2016d)
2013–05	Jul 4–25	50	4	*1, 2, 3, 4, 5*	Cooper et al. (2016b)
2014–12	Jul 4–23	47	5	*1, 2, 3, 4, 5*	Cooper et al. (2016c)
2015–07	Jul 4–25	54	5	*1, 2, 3, 4, 5*	Cooper et al. (2016d)
2016–17	Jul 2–21	48	4	*1, 2, 3, 4, 5*	Cooper et al. (2017)

[a] Cruise IDs were designated by the Department of Fisheries and Oceans Canada.
[b] Bolded and italicized numbers represent regions where productivity experiments were conducted.
[c] This cruise was part of the Bering Strait Environmental Observatory program.
[d] This cruise was conducted as part of the International Polar Year – Canada's Three Oceans project (see Varela et al., 2013 and Wyatt et al., 2013 for further details).

2.2. Seawater sampling

At every CTD/rosette station (Table 1), water column profiles of physical parameters were collected with a CTD profiler (Seabird SB911 +) equipped with sensors for salinity (S), temperature (T), pressure, *in vivo* fluorescence, and photosynthetically active radiation. Seawater samples were collected with 10-L Niskin bottles, which were part of the 24-bottle rosette sampling system that included the CTD.

At primary productivity stations (Table 2), seawater samples were collected at six depths corresponding to light levels of 100%, 55%, 30%, 15%, 1% and 0.1% of the surface incident irradiance (I_o). Seawater for 100% I_o was collected at a 'surface' depth of 1–2 m. At each light level, we measured dissolved nitrate (NO_3^-), total and size-fractionated phytoplankton biomass (as Chl *a*), and ^{13}C and $^{15}NO_3^-$ utilization rates (ρC and ρNO_3).

2.3. Dissolved nutrients

Samples for NO_3^- concentrations were syringe-filtered through precombusted 0.7 μm glass fibre filters and collected in acid-washed 30-mL

Table 2

Locations of primary productivity stations for each of the eight cruises in the Bering and Chukchi Seas from 2006 to 2016.

Cruise ID (YEAR-ID)	Date	Station	Latitude (ºN)	Longitude (ºW)	Bottom Depth (m)	Euphotic Zone Depth, Z_{eu}[b] (m)	DBO Region
2006–01	13 Jul	BCS-6	64.044	171.841	49	36	1[c]
	16 Jul	BRS-4a	65.670	168.341	50	40	2[c]
	18 Jul	PH-2	68.093	168.369	57	27	3W
	19 Jul	M05-04	70.644	168.244	45	30	4[c]
2008–02	16 Jul	SLIP-4	63.026	173.456	74	59	1
	17 Jul	UTBS-1	64.990	169.140	49	44	2
	19 Jul	UTN-4	67.504	168.903	51	42	3W
	20 Jul	CCL-4	69.991	168.020	50	30	4[c]
	21 Jul	BC-2	71.414	157.497	127	44	5
2011–18	15 Jul	SLIP-4	63.030	173.460	71	37	1
	16 Jul	UTBS-1	64.990	169.139	48	32	2
	17 Jul	UTN-4	67.500	168.909	49	20	3W
2012–09	14 Jul	SLIP-4	63.030	173.460	73	40	1
	15 Jul	UTBS-4	64.961	169.885	50	30	2
	17 Jul	SEC-5	68.131	167.510	55	30	3E
2013–05	14 Jul	SLIP-4	63.030	173.460	71	48	1
	15 Jul	UTBS-1	64.992	169.139	49	42	2
	19 Jul	UTN-4	67.500	168.943	51	22	3W
	22 Jul	DBO4.4	71.360	163.028	45	22	4
2014–12	15 Jul	SLIP-4	63.030	173.460	71	46	1
	16 Jul	UTBS-1	64.991	169.141	48	38	2
	17 Jul	UTN-4	67.501	168.904	50	36	3W
	18 Jul	SEC-5	68.128	167.495	50	39	3E
	20 Jul	DBO4.3	71.233	162.635	46	37	4
2015–07	15 Jul	SLIP-4	63.030	173.461	74	67	1
	16 Jul	UTBS-1	64.991	169.141	48	25	2
	17 Jul	UTN-4	67.500	168.942	49	26	3W
	19 Jul	DBO4.4	71.362	163.031	44	38	4
	20 Jul	BarC-5	71.410	157.491	125	29	5
2016–17	13 Jul	SLIP-4	63.030	173.461	72	67	1
	14 Jul	UTBS-1	64.991	169.141	49	44	2
	16 Jul	UTN-4	67.500	168.942	50	25	3W
	18 Jul	DBO4.2	71.102	162.275	49	39	4

[a] Cruise IDs were designated by the Department of Fisheries and Oceans Canada and correspond to Year-ID.
[b] The euphotic zone extends from the ocean surface to the 0.1% incident surface irradiance (I_o) level. Euphotic zone depth (Z_{eu}) corresponds to the 0.1% I_o depth.
[c] In 2006 and 2008, cruises were not conducted as part of the DBO, therefore sampling stations were not always located within each specified DBO region. Stations where sampling occurred near (but not exactly within) the five DBO regions were included within the closest DBO region.

polypropylene bottles. Samples were immediately frozen at $-20\,°C$ until analysis on shore using an Astoria Nutrient Autoanalyzer and following the protocols of Barwell-Clarke and Whitney (1996). Dissolved inorganic carbon (DIC) samples were collected near the surface (5 m) and 5 m from the bottom in 500-mL borosilicate bottles. Samples were preserved with 200 μL of a saturated mercuric chloride solution, stored at $4\,°C$, and analyzed at the Institute of Ocean Sciences (Fisheries and Oceans Canada; Sidney, BC) using a SOMMA-Coulometer system following the methods of Dickson and Goyet (1994). DIC concentrations at the remaining sampling depths were estimated by interpolation using seawater density, and these values were used in the calculation of ρC.

2.4. Total and size-fractionated phytoplankton biomass (Chl a)

Seawater (0.5 L) was sequentially filtered through 5 μm pore-size polycarbonate filters and 0.7 μm pore-size glass fibre filters for analysis of size-fractionated Chl *a*. Prior to 2013, an additional seawater sample (0.5 L) for total Chl *a* was filtered through a 0.7 μm pore size glass fibre filter. After 2013, total Chl *a* was calculated as the sum of the two size fractions. Samples were stored frozen at $-20\,°C$ until analysis ashore. The filtered Chl *a* was extracted with 90% acetone at $-20\,°C$ for 24 h in the dark, measured on a Turner Designs 10 AU fluorometer, and corrected for phaeopigment interference following Parsons et al. (1984).

2.5. Phytoplankton taxonomy

Phytoplankton taxonomic analyses were conducted in 2013. Seawater samples (125 mL) were collected in amber high-density polyethylene bottles at the depth of the Chl *a* maximum, or near the surface (5 m) if no Chl *a* maximum was evident. Samples were fixed with acidic Lugol's solution, and stored in the dark at room temperature (Parsons et al., 1984) until analysis. Due to logistical constraints, phytoplankton identification in DBO1 and DBO2 was only carried out at stations located near (but not within) these regions (i.e. BCL-6a for DBO1 and BRS-3 for DBO2). For DBO3-DBO5, samples were analyzed from both the productivity stations and all other CTD/rosette stations. Prior to microscopic identification, samples were settled for 24 h using 10-mL Utermöhl sedimentation chambers. Phytoplankton cells were enumerated following the Utermöhl (1958) technique and using an inverted microscope equipped with phase and interference (Nomarski) contrasts. Cells were identified to genus/species level, and abundances for each taxon were expressed as number of cells per litre of seawater. The presence or absence of chloroplasts was used to differentiate between autotrophic and heterotrophic cells with the exception of undetermined flagellates, which may include some heterotrophic taxa.

Phytoplankton were further categorized into major taxonomic groups and the total abundance for each group was calculated. These groups are Diatoms (Bacillariophyceae), Dinoflagellates (Dinophyceae), Coccolithophores (Prymnesiophyceae), Phaeocystis (Prymnesiophyceae), Cryptomonads (Cryptophyceae), Chrysophytes (Chrysophyceae), Prasinophytes (Prasinophyceae), Chlorophytes (Chlorophyceae), and undetermined flagellates of likely different taxonomic affinities that were separated into three size classes: $< 3\,\mu m$, between $3\,\mu m$ and $7\,\mu m$, and $> 7\,\mu m$.

2.6. Sea-ice concentrations

Sea-ice concentration data, used to interpret phytoplankton taxonomy for July 2013, were retrieved in May 2017 from the Integrated Climate Date Center (http://icdc.zmaw.de/) at the University of Hamburg (Hamburg, Germany). Sea-ice concentrations were calculated by applying the ARTIST sea-ice (ASI) algorithm to brightness temperatures from the Advanced Microwave Scanning Radiometer on board the EOS (AMSR-E) satellite. A three-day mean of sea-ice concentrations (including the entire sampling date and 2 days prior to sampling) was calculated to account for short-term changes in the amount of sea ice.

2.7. Carbon and nitrate utilization rates, new production, and f-ratios

Carbon and NO_3^- utilization rates were measured using a ^{13}C-$^{15}NO_3^-$ dual tracer method (Dugdale and Goering, 1967; Slawyk et al., 1977). Seawater was collected in 1-L acid-cleaned polycarbonate bottles and enriched with ^{13}C-labeled $NaHCO_3$ (99 atom % ^{13}C, Cambridge Isotope Laboratories) and ^{15}N-labeled $NaNO_3$ (98 atom % ^{15}N, Cambridge Isotope Laboratories) as soon as possible after collection. Isotopic ^{13}C and $^{15}NO_3^-$ additions were made at $\leq 10\%$ of the measured DIC and NO_3^- concentrations, respectively. Sample bottles were placed in acrylic tubes covered with neutral density and blue-coloured photographic film to simulate the *in situ* irradiance level and wavelengths at the sampling depths. Samples were then incubated for 24 h in on-deck acrylic tanks, which were temperature-controlled by using flowing surface seawater. Experiments were terminated by gentle vacuum filtration onto precombusted 0.7 μm glass-fibre filters that were then dried at $60\,°C$ and stored in a desiccator until analysis ashore. The total particulate C (PC) and N (PN) and isotopic composition (^{12}C:^{13}C and ^{14}N:^{15}N) were measured using an Elementar Vario EL Cube elemental analyzer interfaced to a PDZ Europa 20–20 isotope ratio mass spectrometer at the Stable Isotope Facility at the University of California Davis.

Carbon utilization rates (referred as 'primary productivity' in this paper, ρC) were calculated following Hama et al. (1983), while NO_3^- utilization rates (ρNO_3) were calculated using equations (6) and (3) of Dugdale and Wilkerson (1986). When ambient concentrations of NO_3^- were below the detection limit (0.1 μmol L^{-1}), a value equal to the NO_3^- detection limit was used to calculate ρNO_3. Therefore, under those conditions, ρNO_3 represent a potential maximum value of ρNO_3. We estimated the error associated with our measurements of ρC to be $\pm 20\%$ and of ρNO_3 to be $\pm 18\%$, based on the mean relative standard deviation of triplicate measurements conducted every year from 2011 to 2016 (n = 54).

New primary production in C-based units (New-Prod) was estimated by multiplying ρNO_3 by the ratio of PC:PN measured at the end of the incubation for each sample. The proportion of total primary productivity attributable to new primary production was also calculated using these C-based estimates as the *f*-ratio $= (\rho NO_3 \times PC/PN) / \rho C$.

2.8. Data organization and analysis

Primary productivity data were depth-integrated using trapezoidal integration from the surface to the bottom of the euphotic zone (0.1% of surface irradiance). While ρC data from each depth is expressed in molar units, depth-integrated ρC and New-Prod are expressed in units of g C m^{-2} d^{-1} using a conversion of 12 g C mol^{-1} to better compare with published results. Figs. 1, and 5–7 were created using Ocean Data View version 4.7.9 (Schlitzer, R., Ocean Data View, http://odv.awi.de, 2012). Matlab R2014b was used to conduct all statistical tests and significance was determined at $p < 0.05$.

3. Results

3.1. Time-averaged nitrate concentrations, phytoplankton biomass, and utilization of C and NO_3^-

3.1.1. Vertical distributions

Concentrations of NO_3^- increased with depth in the five DBO regions (Fig. 2a) from 2006 to 2016, with the exception of DBO3E (station SEC-5). Station SEC-5, located in the eastern sector of DBO3 and close to the Alaska coastline, was characterized by much lower and invariable $[NO_3^-]$ throughout the water column. The highest $[NO_3^-]$ in the upper euphotic zone (100%, 55% and 30% I_o) occurred in DBO2 and DBO3W. The time-averaged $[NO_3^-]$ showed less vertical variation in these regions compared to DBO1 and DBO4–5, although there was still a small increase with depth. DBO2 had the broadest range of $[NO_3^-]$ for the 10-year period, spanning from undetectable to 18 μmol L^{-1} at the surface,

a

b
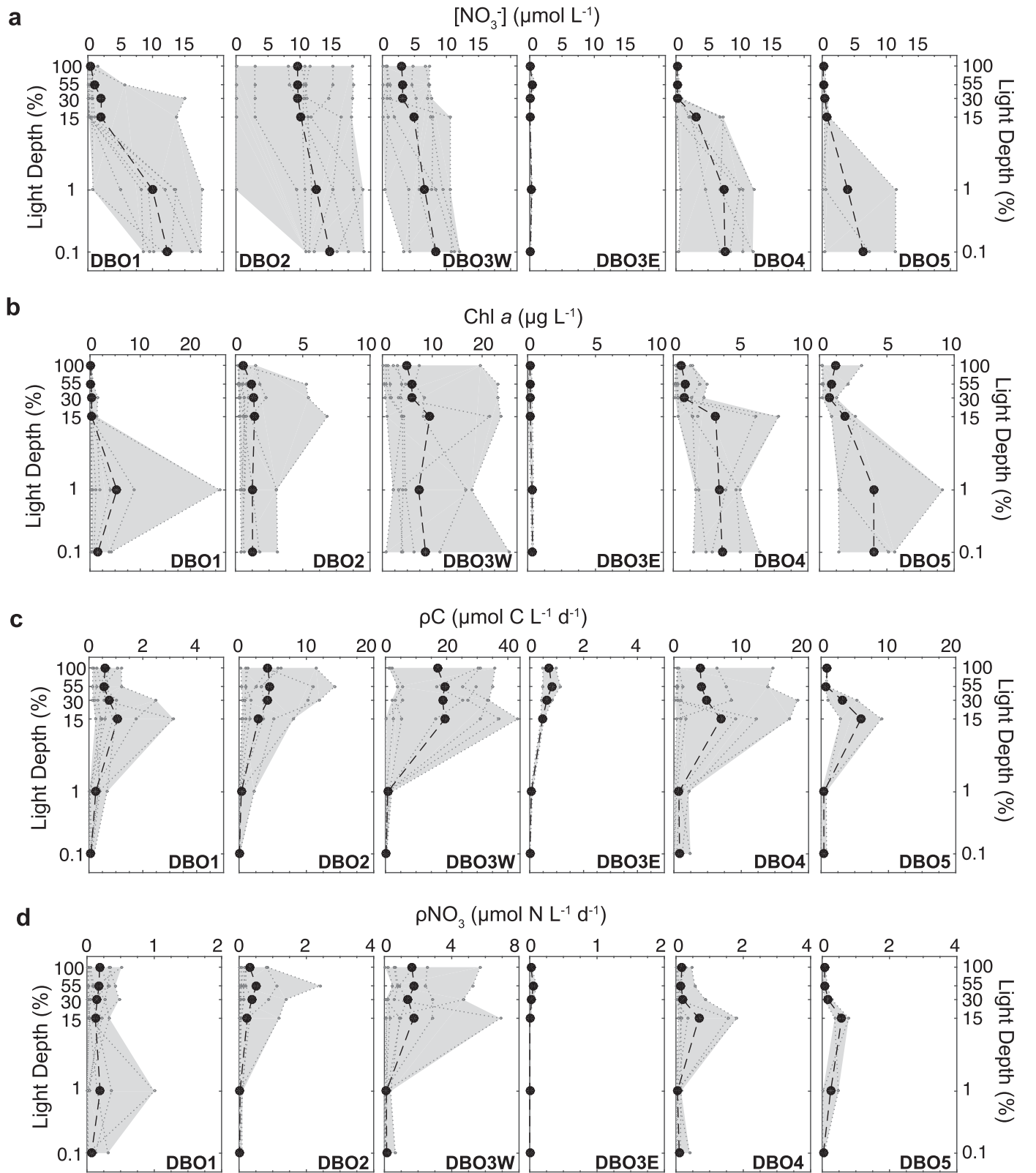

c

d

Fig. 2. Time-averaged vertical profiles of (a) NO_3^- concentration, (b) total Chl *a* concentration, (c) C utilization rate, ρC, and (d) NO_3^- utilization rate, ρNO_3, over the 2006–2016 period for each DBO region. Data are plotted against light depths (i.e. percentage of incident surface irradiance, I_o) to account for differences in depths sampled among years. The y-axis depth scale is logarithmic to reflect the exponential attenuation of irradiance in the water column. Filled black dots and black dashed lines represent the time-averaged vertical profiles, calculated as the average of all years sampled for each light depth. Smaller grey dots and grey dotted lines represent vertical profiles from each year sampled. Note that DBO3E and DBO5 were only sampled on two out of the eight cruises. Shaded grey areas indicate the range of values (maximum and minimum) for each parameter in each region. Profiles from the DBO3 region are separated into west and east sectors (DBO3W and DBO3E, respectively), which are influenced by different water masses (DBO3W = nutrient rich AW/BSW; DBO3E = nutrient poor ACW). Note the different horizontal scales (x-axis) among DBO regions in panels b to d.

and from 12 to 20 μmol L^{-1} at 0.1% I_o. In DBO1–2 and DBO3W, the bottom of the euphotic zone (0.1% I_o) generally showed the least variability compared to the rest of the euphotic zone. In contrast, [NO_3^-] in DBO4 and DBO5 were low with reduced interannual variability in the upper euphotic zone (100%, 55% and 30% I_o), and higher and more variable interannually in the lower euphotic zone (15%, 1% and 0.1% I_o).

The 10-yr time-averaged Chl *a* concentrations were lower in the upper euphotic zone (100%, 55% and 30% I_o) compared to the lower euphotic zone (15%, 1% and 0.1% I_o; Fig. 2b). An exception was DBO3E (Fig. 2b) that showed low values and little variation with depth, similar to [NO_3^-] (Fig. 2a). Subsurface Chl *a* maxima were observed in DBO1, DBO3W, DBO4 and DBO5. These subsurface maxima typically occurred at either 15 or 1% I_o and corresponded to an increase in [NO_3^-]. DBO3W exhibited the highest Chl *a* of all regions, as well as the most interannual variability, while DBO3E showed the lowest Chl *a* and least variability. Chl *a* in DBO1 also showed relatively low interannual variability at all light depths except at 1% I_o. At this depth, Chl *a* was at least 2–3 times higher and showed much more interannual variability (0.25 – 25.8 μg L^{-1}) than the other depths.

Vertical profiles of ρC (Fig. 2c) and ρNO_3 (Fig. 2d) averaged over the 10-yr study exhibited similar spatial trends for the five DBO regions. Both ρC and ρNO_3 were much lower in DBO1 (note different scale for DBO1 for Fig. 2c-d) and in DBO3E compared to the other regions. DBO3E exhibited the lowest ρC and ρNO_3 for the entire DBO region, while ρC and ρNO_3 in DBO3W were the highest (note different scale for DBO3W for Fig. 2c-d). In all regions, ρC decreased to < 1 μmol C L^{-1} d^{-1} (< 12 mg C m^{-3} d^{-1}), and ρNO_3 decreased to < 0.2 μmol N L^{-1} d^{-1} below 15% I_o. Both ρC and ρNO_3 exhibited higher interannual variability at depths above 1% I_o for all regions except for DBO1 and DBO3E. In DBO1, ρNO_3 showed slightly more interannual variability at 1% I_o, as it was also observed for Chl *a*.

3.1.2. Depth-integrated distributions

The high spatial and temporal variabilities observed in the vertical profiles were also reflected in the depth-integrated distributions of [NO_3^-], Chl *a*, ρC and ρNO_3. Depth-integrated [NO_3^-] were generally highest in DBO1 and DBO2, lowest in DBO3E, and intermediate in DBO3W, DBO4 and DBO5 (Table 3; Fig. 3a). There were no obvious temporal trends for [NO_3^-] in any of the DBO regions (Table 3). Depth integrated [NO_3^-] in DBO3E was relatively invariable between years, while interannual variability in [NO_3^-] was much higher for the other DBO regions (Table 3, Fig. 3a).

Depth-integrated Chl *a* distributions and the percent contribution of > 5 μm Chl *a* to total Chl *a* were generally highest in DBO3W, lowest in DBO3E, and in between these two extremes for the other DBO regions (Table 3; Fig. 3b-c). Chl *a* > 5 μm contributed more than 40% to total Chl *a* in all regions, except for DBO3E where it accounted for only ~30% of total Chl *a* (Table 3, Fig. 3c). Higher total Chl *a* in DBO3W coincided with a greater contribution of the > 5 μm size fraction (r = 0.56, *p* < 0.003). Interannual variability was highest in DBO1-2 and DBO3W for total Chl *a,* and there were no clear year-to-year trends in any of the DBO regions. The same was true for the percent contribution of > 5 μm cells to total Chl *a* in all DBO regions except for DBO1, where a significant decreasing trend (r = -0.94, *p* < 0.02) was calculated from 2012 to 2016 (Table 3).

Depth-integrated ρC and ρNO_3 exhibited similar spatial variations to Chl *a*, with the highest and lowest values occurring in DBO3W and DBO3E, respectively, while values for the other DBO regions fell between those in DBO3W and E (Table 3; Fig. 4a-b). There were no consistent trends with time anywhere, but DBO1, DBO3E and DBO5 were less variable than the other regions (Table 3). Although ρC showed similar spatial variations to ρNO_3, ρNO_3 and ρC were only weakly correlated with each other (r = 0.33, *p* = 0.10).

3.1.3. New primary production and f-ratios

Depth-integrated New-Prod followed similar spatial trends to Chl a, ρC and ρNO_3, with rates being highest in DBO3W, lowest in DBO3E and intermediate for the other DBO regions (Table 3; Fig. 4c). Rates of New-Prod were highly variable between years in DBO1-2, DBO3W and DBO4, with no consistent trends with time (Table 3). Depth integrated *f*-ratios were highly variable from year to year, while, when averaged over the entire study period, *f*-ratios were similar for all DBO regions except for DBO3E (Table 3; Fig. 4d). In addition, little can be said for the *f*-ratios in the DBO1 region, as values were often greater than 1. An *f*-ratio > 1 is not realistic given that 1 represents 100% of the productivity resulting from NO_3^- utilization and potentially available for export. These high *f*-ratios are likely a result of calculation artefacts by using the ratio of ρNO_3 to ρC, rather than a more accurate *f*-ratio of N-based utilization rates (i.e. ρNO_3/ (ρNH_4 + ρUrea + ρNO_3)). Therefore, the *f*-ratios presented for DBO1 in Table 3 and Fig. 4d should be interpreted with caution.

3.1.4. Statistical comparisons among DBO regions and years

Statistical differences in depth-integrated [NO_3^-], Chl *a*, ρC, ρNO_3, New-Prod and *f*-ratios grouped either by region or by year were determined using a nonparametric Kruskal-Wallis test with post hoc comparison (at *p* < 0.05). When data were grouped by DBO region, significant differences were observed between DBO3W and E for depth-integrated Chl *a*, ρC, ρNO_3 and New-Prod, and between DBO1 and DBO3W for depth-integrated ρC. No significant differences occurred between any of the combinations of DBO2, DBO4 or DBO5 for any of the parameters measured. If data were grouped geographically into either the Bering Sea (DBO1 and DBO2) or the Chukchi Sea (DBO3 to 5), significant differences occurred between the Bering and Chukchi Seas for depth-integrated [NO_3^-], Chl *a*, ρC and New-Prod. With the exception of New-Prod, the differences between the Bering and Chukchi Seas remained significant regardless of whether or not the data from DBO3E were included in the Chukchi Sea group. When data were instead grouped by year, no significant differences between years occurred regardless of how the data were grouped, i.e. by station, by DBO region, by water mass (i.e. separating DBO3 into east and west) or by geography (i.e. Bering Sea or Chukchi Sea). It is possible that the lack of significant yearly differences results from a low ratio of observational frequency to natural variability.

3.1.5. Correlation analysis between physical and biological parameters in the Bering and Chukchi Seas

To identify potential environmental controls on phytoplankton biomass and productivity, we conducted a correlation analysis between euphotic-zone integrated [NO_3^-], phytoplankton biomass, primary productivity, and several physical parameters (Table 4). Data were grouped into either Bering Sea (DBO1-DBO2) or Chukchi Sea (DBO3-DBO5) regions, and a separate analysis was conducted for each of the two regions (Bering and Chukchi). Significant (*p* < 0.05) correlations between parameters were found in both the Bering and Chukchi Seas.

In the Bering Sea, only the depth of the euphotic zone (Z_{eu}) and [NO_3^-] showed any correlation with physical parameters, with Z_{eu} being negatively correlated with bottom temperature (i.e. Z_{eu} was deeper when bottom temperatures were lower/colder), and [NO_3^-] being positively correlated with both surface and bottom salinity. In contrast, a number of biological parameters were significantly correlated with each other. Total Chl *a* was positively correlated with the > 5 μm and < 5 μm Chl *a* size fractions, as well as with New-Prod and the *f*-ratio, while Chl *a* > 5 μm was positively correlated with New-Prod. In addition, ρC was positively correlated with ρNO_3 and New-Prod, while ρNO_3, New-Prod and the *f*-ratio were all positively correlated with each other.

In the Chukchi Sea, no significant correlations were found between any biological and physical parameters; however, like for the Bering Sea, a number of significant correlations were found between biological

Table 3

Depth-integrated measurements of nitrate (NO_3^-) and chlorophyll *a* (Chl *a*) concentrations, the percent contribution of > 5 μm Chl *a*, primary productivity (ρC), nitrate utilization rates (ρNO_3), new production and *f*-ratios for the five DBO regions in the Bering and Chukchi Seas in July from 2006 to 2016. Data from DBO3 is split into the western (DBO3W) and eastern (DBO3E) sectors due to differences in the water mass composition (AW/BSW and ACW, respectively). Depth integrations were done from the ocean surface to the 0.1% I_o depth. (-) indicates that no data are available. Values listed as < 1.6 mmol m^{-2} for [NO_3^-] represent stations where [NO_3^-] at all depths sampled were below the analytical detection limit (< 0.1 μmol L^{-1}).

Region	Year	[NO_3^-] (mmol m^{-2})	Chl *a* (mg m^{-2})	Chl *a* > 5 μm (%)	ρC (g C m^{-2} d^{-1})	ρNO_3 (mmol N m^{-2} d^{-1})	New Production (g C m^{-2} d^{-1})	*f*-ratio
Northern Bering Shelf								
DBO1	2006	437	46.1	–	0.65	5.37	0.44	0.67
	2008	568	17.6	44.3	0.17	7.37	0.45	> 1
	2011	79.8	23.5	–	0.19	6.41	0.53	> 1
	2012	153	98.7	88.4	0.13	3.01	0.21	> 1
	2013	168	331	68.1	0.44	10.4	0.97	> 1
	2014	91.1	47.4	76.6	0.66	14.9	0.87	> 1
	2015	165	7.4	61.3	0.25	0.97	0.09	0.35
	2016	337	13.3	32.0	0.21	1.94	0.18	0.57
Mean (± SE)		250 ± 62.9	73.1 ± 38.3	61.8 ± 8.5	0.34 ± 0.08	6.30 ± 1.64	0.47 ± 0.11	0.53 ± 0.09[a]
DBO2	2006	< 1.6	17.2	–	0.17	0.40	0.03	0.18
	2008	502	21.4	47.5	0.97	2.96	0.15	0.18
	2011	144	149	–	2.19	28.9	2.09	0.99
	2012	524	31.0	92.9	0.23	4.89	0.29	> 1
	2013	501	14.0	61.8	0.24	1.45	0.11	0.45
	2014	522	81.4	91.2	2.74	15.3	0.97	0.38
	2015	403	17.8	27.9	0.63	1.6	0.12	0.19
	2016	406	19.7	43.5	0.83	1.98	0.13	0.19
Mean (± SE)		429 ± 51.3	43.9 ± 16.9	60.8 ± 10.8	1.00 ± 0.34	7.19 ± 3.53	0.49 ± 0.25	0.37 ± 0.11
Southeastern Chukchi Sea								
DBO3W	2006	39.6	77.2	–	0.44	1.58	0.12	0.26
	2008	323	40.2	72.5	1.03	95.5	5.27	> 1
	2011	141	141	–	4.46	35.3	4.70	0.88
	2012	–	–	–	–	–	–	–
	2013	123	233	95.7	3.66	17.7	0.82	0.40
	2014	157	128	88.6	1.32	7.85	0.65	0.48
	2015	226	71.8	65.2	4.96	36.7	3.25	0.64
	2016	19.9	510	90.2	7.94	13.5	1.56	0.21
Mean (± SE)		147 ± 39.5	172 ± 61.2	82.4 ± 5.79	3.40 ± 1.01	29.7 ± 12.0	2.34 ± 0.78	0.48 ± 0.10
DBO3E	2006	–	–	–	–	–	–	–
	2008	–	–	–	–	–	–	–
	2011	–	–	–	–	–	–	–
	2012	5.00	5.01	33.3	0.07	0.08	0.01	0.08
	2013	–	–	–	–	–	–	–
	2014	6.38	14.0	32.9	0.22	0.54	0.04	0.23
	2015	–	–	–	–	–	–	–
	2016	–	–	–	–	–	–	–
Mean (± SE)		5.69 ± 0.69	9.51 ± 4.50	33.1 ± 0.20	0.15 ± 0.08	0.31 ± 0.23	0.03 ± 0.02	0.16 ± 0.08
Northeastern Chukchi Sea								
DBO4	2006	76.9	114		0.95	4.32	0.40	0.40
	2008	172	54.4	89.5	1.15	27.9	2.33	> 1
	2011	–	–	–	–	–	–	–
	2012	–	–	–	–	–	–	–
	2013	6.29	63.2	61.2	2.87	3.45	0.17	0.17
	2014	183	39.9	73.7	0.31	3.58	0.27	> 1
	2015	194	98.6	90.2	1.44	12.5	1.09	0.75
	2016	149	38.2	67.9	0.32	1.29	0.11	0.33
Mean (± SE)		130 ± 30.1	68.1 ± 12.8	76.5 ± 5.80	1.17 ± 0.39	8.84 ± 4.13	0.73 ± 0.35	0.41 ± 0.12
DBO5	2006	–	–	–	–	–	–	–
	2008	248	60.7	88.5	1.58	11.1	0.85	0.50
	2011	–	–	–	–	–	–	–
	2012	–	–	–	–	–	–	–
	2013	–	–	–	–	–	–	–
	2014	–	–	–	–	–	–	–
	2015	37.9	40	73.0	0.40	6	0.54	> 1
	2016	–	–	–	–	–	–	–
Mean (± SE)		143 ± 105	50.4 ± 10.4	80.8 ± 7.75	0.99 ± 0.59	8.55 ± 2.55	0.70 ± 0.16	0.50

[a] the mean f-ratio was only calculated from years where the f-ratio was < 1.

parameters. For example, [NO_3^-] was positively correlated with Z_{eu}, ρNO_3, New-Prod and the *f*-ratio. Total Chl *a* and Chl *a* > 5 μm were positively correlated with each other and with ρC, while ρC was also negatively correlated with Z_{eu}. Similar to the Bering Sea, ρNO_3, New-Prod and the *f*-ratio in the Chukchi Sea were all positively correlated with each other.

3.2. Phytoplankton assemblage composition

Phytoplankton taxonomic analysis was only conducted in 2013 at the depth of the Chl *a* maximum (or at 5 m if no Chl *a* maximum was identified) (Figs. 5 and 6). For each DBO region, with the exception of DBO3, the average proportion of cell numbers from each taxonomic group was calculated using data from all CTD/rosette and primary
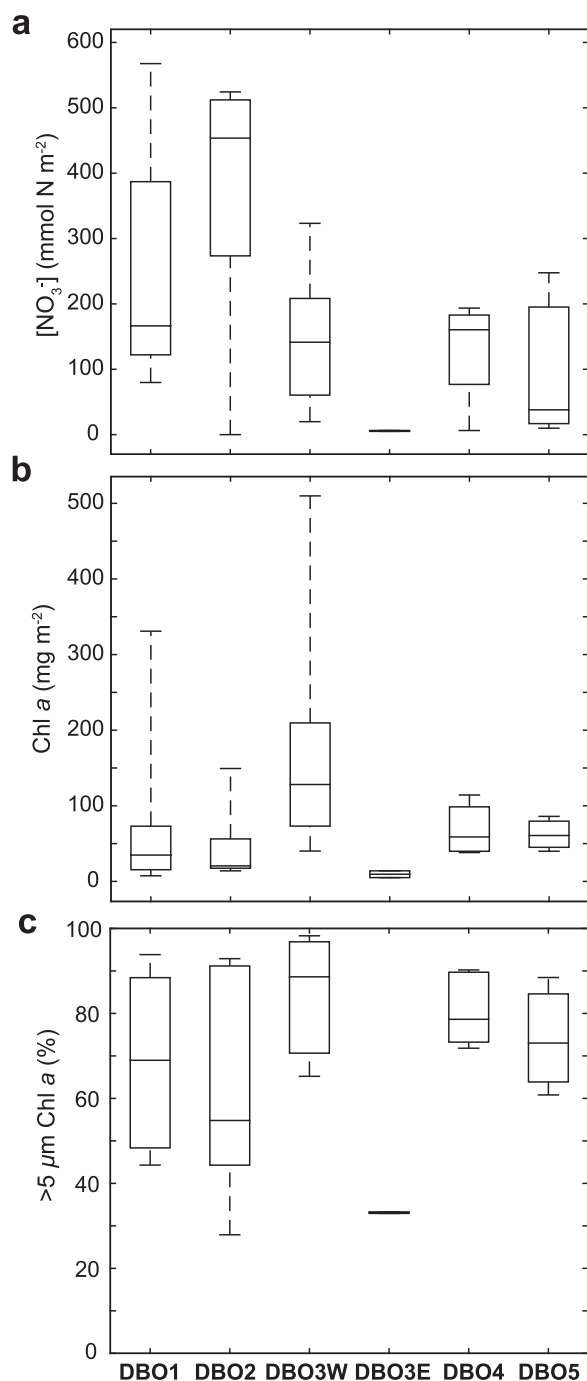
Fig. 3. Box plots of time-averaged depth-integrated (a) NO_3^- concentration, (b) total Chl *a* concentration, and (c) percent contribution of > 5 μm Chl *a* to total Chl *a* for each DBO region from 2006 to 2016. Depth integrations were done from the ocean surface to the 0.1% I_o depth. The horizontal line in the middle of each box represents the median, and the top and bottom of the boxes represents the 25th and 75th percentiles, respectively. The whiskers extending above and below each box extend to the maximum and minimum measured values, respectively. Data from the DBO3 region are separated into west (DBO3W) and east (DBO3E) as in Fig. 2.

productivity stations within each region (Fig. 5a). In DBO3, stations were further separated into DBO3E (SEC-5 to SEC-8) and DBO3W (UTN-1 to UTN-7, and SEC-1 to SEC-2) (Fig. 5a). Diatoms dominated the phytoplankton assemblages in all of the DBO regions with the exception of DBO3E where coccolithophores and small flagellates (< 7 μm) were dominant (Fig. 5b).

Spatial variations in total phytoplankton abundance were primarily driven by the contribution of diatoms (r = 0.92, *p* < 0.01), but also correlated with the amount of sea ice cover (r = 0.65, *p* < 0.01; Fig. 6a-b). The highest total cell abundance ($\sim 4 \times 10^6$ cells L^{-1}) was measured in DBO4 and corresponded to an increase in sea ice cover (Fig. 6a-b). This region also exhibited the largest diversity in phytoplankton assemblage composition, although diatoms were still the most abundant. *Phaeocystis* spp. reached up to $\sim 1.3 \times 10^6$ cells L^{-1} at DBO4.3, and was also present at some stations in the DBO3 and DBO5 regions, but was not observed in DBO1 or DBO2. Flagellates were present at all stations, but their abundance was spatially variable. Larger (> 7 μm) unidentified flagellates were most abundant in DBO4 (Fig. 6b), while smaller (3–7 μm) unidentified flagellates did not exhibit much spatial variability, with an average abundance of $\sim 0.08 \times 10^6$ cells L^{-1} for all stations. The lowest total phytoplankton abundance of $\sim 0.15 \times 10^6$ cells L^{-1} was observed at stations near the southernmost edge of DBO3 (UTN-1 and UTN-2) and at BarC-1 in DBO5, although diatoms were still the dominant group at these stations. Coccolithophores were present in the highest numbers at stations with relatively low total abundance ($\sim 0.46 \times 10^6$ cells L^{-1}) in the eastern sector of DBO3 (SEC-5 to SEC-8) near the Alaska coast, reaching a maximum of 0.32×10^6 cells L^{-1} at SEC-6 (Fig. 6b) Autotrophic dinoflagellates were present in consistently low numbers throughout the DBO regions ($0.002 - 0.27 \times 10^6$ cells L^{-1}) with relatively little spatial variation, except for a slight increase at DBO4. The centric diatoms *Chaetoceros* sp. and *Thalassiosira* sp. were the most abundant in all of the DBO regions except for DBO4, where *Fragilariopsis* sp. and other pennate diatom species dominated the assemblages (Fig. 6c-d).

The most commonly observed phytoplankton taxa (i.e. those that were present at 10 or more stations) were small (< 7 μm) flagellates, cryptophytes, prymnesiophytes, and diatoms (Table 5). Small (< 7 μm) flagellates, and the diatom *Cylindrotheca closterium* were the only phytoplankton present in all DBO regions, although *Chaetoceros socialis* and *Chaetoceros furcellatus* were observed in all regions except DBO3E and DBO4 respectively. *Cryptomonas* spp. and *Phaeocystis pouchetii* were only found north of the Bering Strait (DBO3-DBO5), although *Cryptomonas* spp. was not found in DBO5. *Phaeocystis pouchetii* was only observed as single cells, not in colonies. Diatoms were the most abundant and diverse in the entire DBO region, with *Thalassiosira nordenskioeldii*, *Fragilariopsis oceanica*, *Cylindrotheca closterium* and spores of *Chaetoceros furcellatus* present at 14-23 stations of the 24 stations analyzed.

4. Discussion

4.1. Regional patterns of summertime nutrient and phytoplankton dynamics in the Pacific Arctic Region from 2006 to 2016

4.1.1. Nutrient and phytoplankton biomass

Our measurements of euphotic zone $[NO_3^-]$ and Chl *a* fell within the range of published summertime values and followed similar spatial trends (e.g. Hansell and Goering, 1990; Springer and McRoy, 1993; Lee et al., 2007, 2012, 2013a; Varela et al., 2013; Danielson et al., 2017). In the Chukchi Sea regions (DBO3–5), both $[NO_3^-]$ and Chl *a* exhibited depth profiles often observed in Arctic marine waters (e.g. Martin et al., 2012; Brown et al., 2015), with $[NO_3^-]$ depleted at the surface and a subsurface Chl *a* maxima (SCM) occurring at the depth where $[NO_3^-]$ increases (with DBO3E as an exception; Fig. 2a-b). Nitrate concentrations increased with depth in all regions except in the eastern sector of DBO3, but the increase was most pronounced in regions farther away from the Bering Strait (i.e. DBO1, DBO4 and DBO5). Similarly, although SCM were generally observed in all regions, this feature was least apparent in DBO2 (near the Bering Strait) and in the eastern sector of DBO3.

The highest $[NO_3^-]$ were usually observed in DBO2 in the Chirikov Basin (Table 3; Fig. 3a), where turbulent mixing brings nutrient-rich bottom waters to the surface (Walsh et al., 1989). Chl *a* concentrations
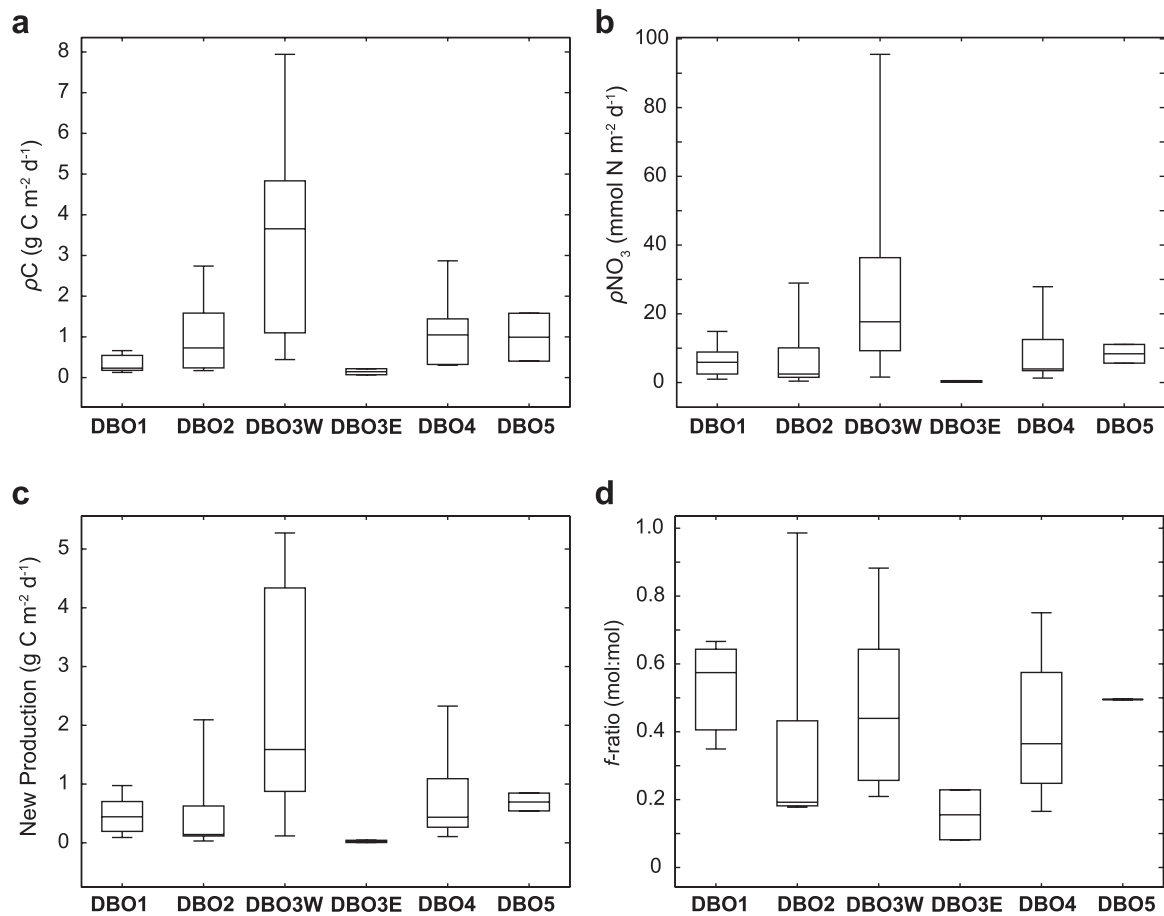
Fig. 4. Box plots of time-averaged depth-integrated (a) C utilization rate, ρC, (b) NO_3^- utilization rate, ρNO3 (c) new production (New-Prod), and (d) *f*-ratios for each DBO region from 2006 to 2016 as in Fig. 3.

in DBO2 were low and invariant throughout the water column, which could be a reflection of our time of sampling given that the seasonal bloom in DBO2 typically occurs when the sea ice retreats earlier in the year (e.g. Springer and McRoy, 1993; Brown et al., 2011). However, given the high $[NO_3^-]$ throughout the water column, the low Chl *a* could be due to turbulent vertical mixing of the water (occurring after sea-ice melt) to below the critical depth. DBO2 had a relatively low stratification index ($\sim$0.5 km m^{-3}, calculated as the difference between densities at the surface and bottom depths) compared to DBO1, DBO4 and DBO5 (1.7–3.3 kg m^{-3}), which confirms that the water column in DBO2 is well mixed. However, while DBO3W had a stratification index the same as that of DBO2 ($\sim$0.5 kg m^{-3}) and similarly high water-column $[NO_3^-]$, the time-averaged Chl *a* in DBO3W was 5–8 times higher throughout the water column compared to DBO2 (Fig. 2b). These results suggest that bottom-up controls, such as mixing alone, cannot explain the low biomass in DBO2. Another possibility is top-down controls, such as grazing by zooplankton. While zooplankton grazing rates are generally low in the PAR compared to other Arctic and global ecosystems (e.g. Campbell et al., 2009; Sherr et al., 2009), grazing by microzooplankton in the Bering Sea has been shown to limit biomass accumulation in the later stages of phytoplankton blooms (Sherr et al., 2013). The differences we observe between DBO2 and DBO3W could also reflect a difference in bloom timing between these regions, with the seasonal bloom in DBO3W occurring later (and thus closer to our sampling time), leaving less time for the zooplankton in this region to respond to the increasing phytoplankton biomass.

While $[NO_3^-]$ was detectable throughout the water column in DBO3W, it was almost undetectable in DBO3E. Chl *a* showed a similar trend, with values significantly lower in the eastern sector of DBO3

compared to the west. This east-west gradient is consistent with previous studies (e.g. Walsh et al., 1989; Cooper et al., 2012; Danielson et al., 2017) and is discussed in more detail in Section 4.2.2. In DBO4 and DBO5, $[NO_3^-]$ and Chl *a* were usually minimal in the upper euphotic zone (100%, 55% and 30% I_o) compared to the lower euphotic zone (15%, 1% and 0.1% I_o). This is indicative of biological utilization of NO_3^- as the waters transit northwards and is reflected in the decreasing euphotic-zone $[NO_3^-]$ throughout the PAR, with $[NO_3^-]$ in the Chukchi Sea regions (DBO3 to DBO5) being about half of those in the northern Bering Sea regions (DBO1 and DBO2).

4.1.2. Primary productivity and nitrate utilization rates

The magnitude of our productivity estimates (ρC and ρNO3) agreed with those in published studies (Table 6), except for ρNO3 in the entire DBO3 region (DBO3E and W combined), where our measurements were 2–4 times higher than those reported previously (Lee et al., 2007, 2013a; Codispoti et al., 2013). This discrepancy is likely because of later sampling times (August) for the Lee et al. (2007, 2013a) studies. The discrepancy with Codispoti et al. (2013) may be driven by the assumed length of the growing season, given that they estimate the length of growing season in the southern Chukchi Sea to range from 40 to 86 days. The value of ρNO3 for the Codispoti et al. study listed in Table 6 is based on an 86-day growing season. Recalculating their estimate of ρNO3 using a shorter, 40-day growing season increases this value from 10.3 to 22.1 mmol N m^{-2} d^{-1}, which is then in good agreement with our own estimate of ρNO3 for DBO3 (Table 6).

Spatial trends were similar for ρC, ρNO3 and New-Prod. The similarity between ρNO3 and New-Prod was primarily due to the relatively consistent PC:PN ratio, which is used for the conversion of ρNO3 to

Table 4
Correlation matrix among physical, chemical and biological parameters for the Bering and Chukchi Seas from 2006 to 2016. Physical data (temperature and salinity) is presented for surface and bottom depths, and biological and chemical data are presented as depth-integrated values from the ocean surface to the 0.1% I_o depth. Significant relationships at $p < 0.05$ and $p < 0.01$ are in bold. Significant relationships at $p < 0.10$ are in italics. Surf = surface (1–2 m), Bot = bottom (2–5 m from the seafloor, T = temperature, S = salinity, Z_{eu} = euphotic zone depth.

	Surf T	Bot T	Surf S	Bot S	Z_{eu} (m)	[NO_3^-]	Chl a	Chl $a > 5\,\mu m$	Chl $a < 5\,\mu m$	ρC	ρNO_3	New-Prod	f-ratio
Bering Sea (DBO1, DBO2)													
Surface T													
Bottom T	− **0.56**[**]												
Surface S	− **0.73**[*]	0.22											
Bottom S	0.00	− 0.07	0.37										
Z_{eu} (m)	0.41	− **0.66**[*]	− 0.06	− 0.18									
[NO_3^-]	− 0.41	0.18	**0.56**[**]	**0.64**[*]	− 0.05								
Chl a	0.18	− 0.25	− 0.27	− 0.08	− 0.09	− 0.28							
Chl $a > 5\,\mu m$	0.31	− 0.30	− *0.53*[†]	− 0.13	− 0.06	− 0.39	**0.998**[*]						
Chl $a < 5\,\mu m$	0.37	− 0.06	− 0.34	0.13	− 0.17	− 0.31	**0.75**[*]	**0.72**[*]					
ρC	− 0.24	0.43	0.15	0.09	− 0.32	0.17	0.23	0.06	0.04				
ρNO_3	− 0.02	− 0.03	− 0.06	0.01	− 0.24	− 0.18	*0.49*[†]	0.44	0.34	**0.72**[*]			
New-Prod	0.01	− 0.05	− 0.13	− 0.03	− 0.24	− 0.23	**0.59**[**]	**0.66**[**]	0.49	**0.68**[*]	**0.98**[*]		
f-ratio	0.21	− 0.31	− 0.37	0.00	− 0.05	− 0.15	**0.74**[**]	0.13	− *0.71*[†]	0.36	**0.74**[**]	**0.78**[*]	
Chukchi Sea (DBO3, DBO4, DBO5)													
Surface T													
Bottom T	**0.65**[*]												
Surface S	**0.65**[*]	**0.78**[*]											
Bottom S	− *0.41*[†]	− **0.52**[**]	− 0.24										
Z_{eu} (m)	0.03	− 0.20	− 0.24	− 0.21									
[NO_3^-]	− 0.02	0.01	0.01	0.21	**0.50**[**]								
Chl a	0.01	0.23	0.34	0.05	− *0.42*	− 0.20							
Chl $a > 5\,\mu m$	0.02	0.25	0.39	0.04	− 0.40	− 0.19	**0.99**[*]						
Chl $a < 5\,\mu m$	− 0.32	0.02	− 0.01	0.25	− 0.41	0.16	− 0.12	− 0.14					
ρC	0.18	*0.41*[†]	0.40	0.22	− **0.57**[**]	− 0.03	**0.83**[*]	**0.83**[*]	0.29				
ρNO_3	0.22	0.34	0.37	0.04	0.11	**0.69**[*]	0.00	− 0.03	0.20	0.20			
New-Prod	0.28	0.43	0.41	0.20	− 0.22	**0.59**[**]	0.12	0.07	0.40	*0.46*[†]	**0.91**[*]		
f-ratio	0.24	0.16	0.09	0.13	0.00	**0.77**[*]	− 0.02	− 0.04	0.37	0.22	**0.76**[*]	**0.75**[*]	

[*] $p < 0.01$.
[**] $p < 0.05$.
[†] $p < 0.10$.

units of C, throughout the study area and period (average ± SD = 6.8 ± 1.4 mol:mol). Distinct subsurface maxima were observed in DBO1 for ρC, and in DBO4 and DBO5 for ρC and ρNO_3. With the exception of DBO1, profiles of ρC and ρNO_3 exhibited similar trends within each region, which suggests that NO_3^- utilization drives primary productivity in these regions. Despite generally high [NO_3^-], productivity was almost undetectable at 1% and 0.1% I_o in all DBO regions, which suggests that light is the limiting factor at these depths. It is possible that the relatively high ammonium concentrations ([NH_4^+]) of ~1–3 $\mu mol\,L^{-1}$ typically found below ~25 m (i.e. 1% and 0.1% I_o) in the PAR (e.g. Lee et al., 2012, 2013a; Danielson et al., 2017) may inhibit ρNO_3 at these depths (e.g. Dortch, 1990; Lomas and Glibert, 1999); however, the fact that ρC is also low suggests that another factor (most likely light), rather than nutrients, may be responsible for the low productivity at 1% and 0.1% I_o.

Latitudinal patterns of primary productivity reflected differences in the timing of the seasonal bloom, which are, in turn, are tied to the timing of the annual sea-ice retreat (Brown et al., 2011; 2013). Sea-ice retreat begins in early May in DBO1 and continues northward as the season progresses (Brown et al., 2011; Frey et al., 2015). By the time of our July sampling in DBO1, the seasonal bloom would have already passed, depleting nutrients in surface waters and resulting in a SCM below the nutricline (e.g. Cooper et al., 2012; Fig. 2a-b). This agrees with our observations of a subsurface Chl a maximum generally at 1% I_o (Fig. 2b), with corresponding, but shallower maximum in ρC at 15% I_o. A subsurface productivity maximum found at shallower depths than the SCM is consistent with previous observations in the PAR (Brown et al., 2015). This difference between the depths of the SCM and productivity maximum could be driven by an adaptation of phytoplankton to lower light levels through an increase in chlorophyll content. This would lead to a decrease in C:Chl a ratios with depth, consistent with that observed

in this study (data not shown) and previously (e.g. Beardall and Morris, 1976; Falkowski et al., 1985). It is also possible that the high phytoplankton biomass observed below the ρC maximum in DBO1 could have been formed farther south, given that waters near the lower limit of the euphotic zone (15–0.1% surface irradiance) in this region also carry the temperature and salinity signature of the cold and saline waters flowing out of the Gulf of Anadyr. These waters transport both nutrients and organic matter northwards from the Pacific, and thus could have contributed to the high biomass concentrations we observe (e.g. Hansell et al., 1989). Nevertheless, it is most likely that the high phytoplankton biomass observed at 1% I_o in DBO1 was produced locally given that both ρC and ρNO_3 were detectable at this depth. Furthermore, years with high euphotic-zone integrated Chl a generally also had high euphotic-zone integrated ρC and ρNO_3 (Table 3). This also suggests that high biomass we observed in DBO1 would have been produced locally and not advected into the region.

In contrast to the presence of a subsurface ρC maximum at 15% I_o, ρNO_3 was relatively low and invariant throughout the water column at DBO1, which also supports the assertion that DBO1 was in a post-bloom condition at the time of our sampling. Differences in the shape of the vertical profiles of ρNO_3 and ρC suggest that phytoplankton growth may have been supported by other, likely regenerated, N sources such as NH_4^+ at least at the depth of the ρC maximum. Ammonium concentrations in the upper (100–30% I_o) and lower (15–0.1% I_o) euphotic zone in DBO1 were ~0.5 $\mu mol\,L^{-1}$ and 1–3 $\mu mol\,L^{-1}$ respectively for our sampling period (Cooper and Grebmeier, 2016a, 2016b; Cooper et al., 2016a, 2016d, 2016b, 2016c, 2017). The low [NO_3^-] in the upper euphotic zone could explain the low ρNO_3 observed at these depths; however, the low ρNO_3 in the lower euphotic zone despite high [NO_3^-] could be due to inhibition of ρNO_3 by NH_4^+ given the higher [NH_4^+] observed at these depths (Dortch, 1990; Lomas and Glibert, 1999;
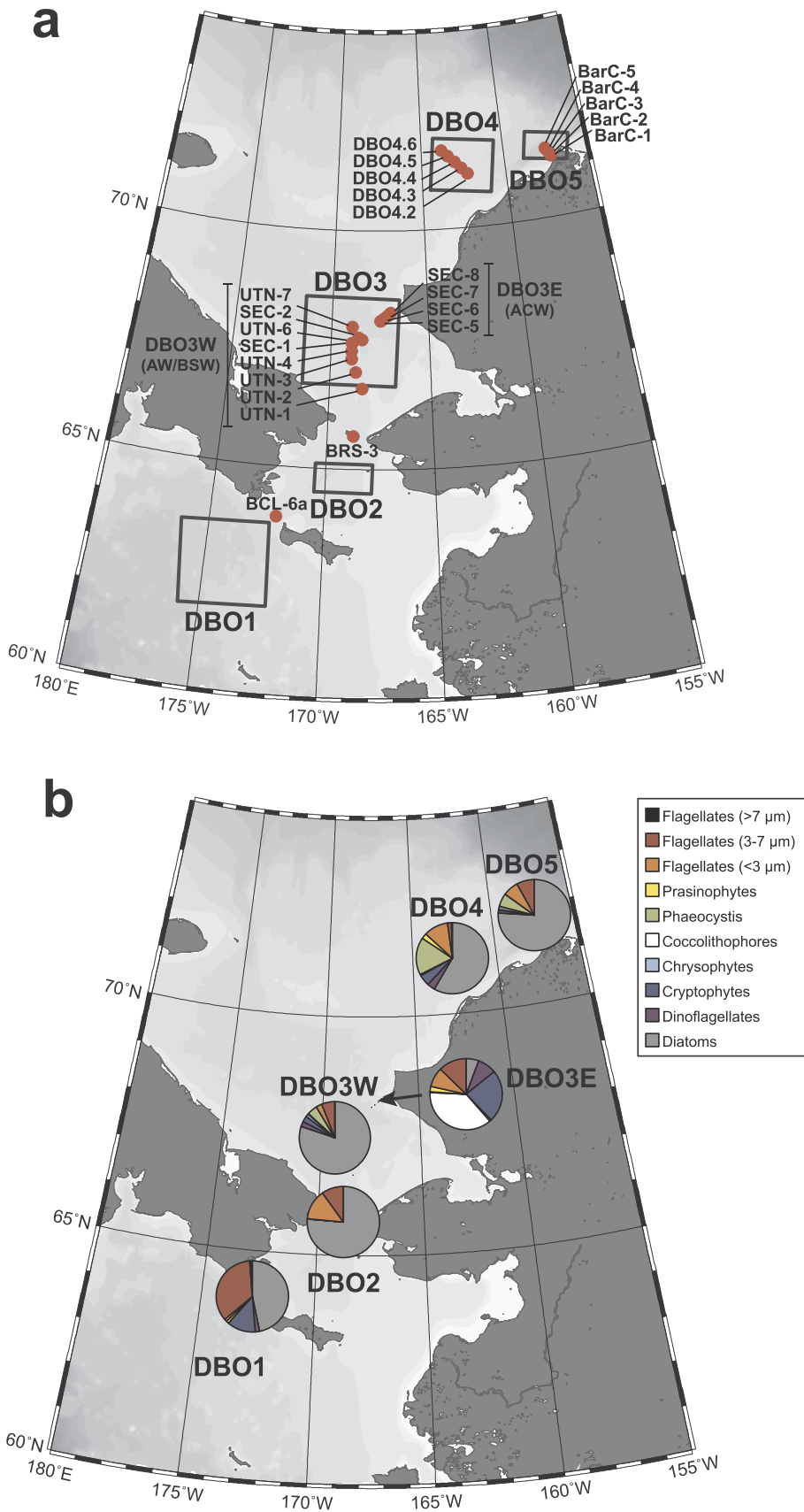
Fig. 5. Station locations and DBO averages for phytoplankton assemblage composition in July 2013. (a) Map of DBO region bounding boxes and station locations where phytoplankton taxonomic identification was conducted at the depth of the chlorophyll maximum (or 5 m depth if maximum was not identified). AW/BSW and ACW refer to the dominant water masses in DBO3W and DBO3E, respectively (Fig. 1a). (b) Proportion of cell numbers from each taxonomic group to total phytoplankton cell numbers averaged for each DBO region. The three size classes of flagellates ($< 3\,\mu m$, $3–7\,\mu m$ and $> 7\,\mu m$) were undetermined species of likely different taxonomic affinities. Data from the DBO3 region are separated into west (DBO3W) and east (DBO3E) as in previous figures. Due to logistical constraints, only samples from stations near (but not within) DBO1 (BCL-6a) and DBO2 (BRS-3) were analyzed for phytoplankton taxonomy.

Varela and Harrison, 1999). Previous work further supports that NH_4^+ may be responsible for reduced ρNO_3, since Lee et al. (2013a) observed high $[NH_4^+]$ and ρNH_4, and low ρNO_3 despite high $[NO_3^-]$ in the lower

euphotic zone in late July in this region, only two weeks after our sampling time.

Primary productivity in DBO2 was relatively low given the high
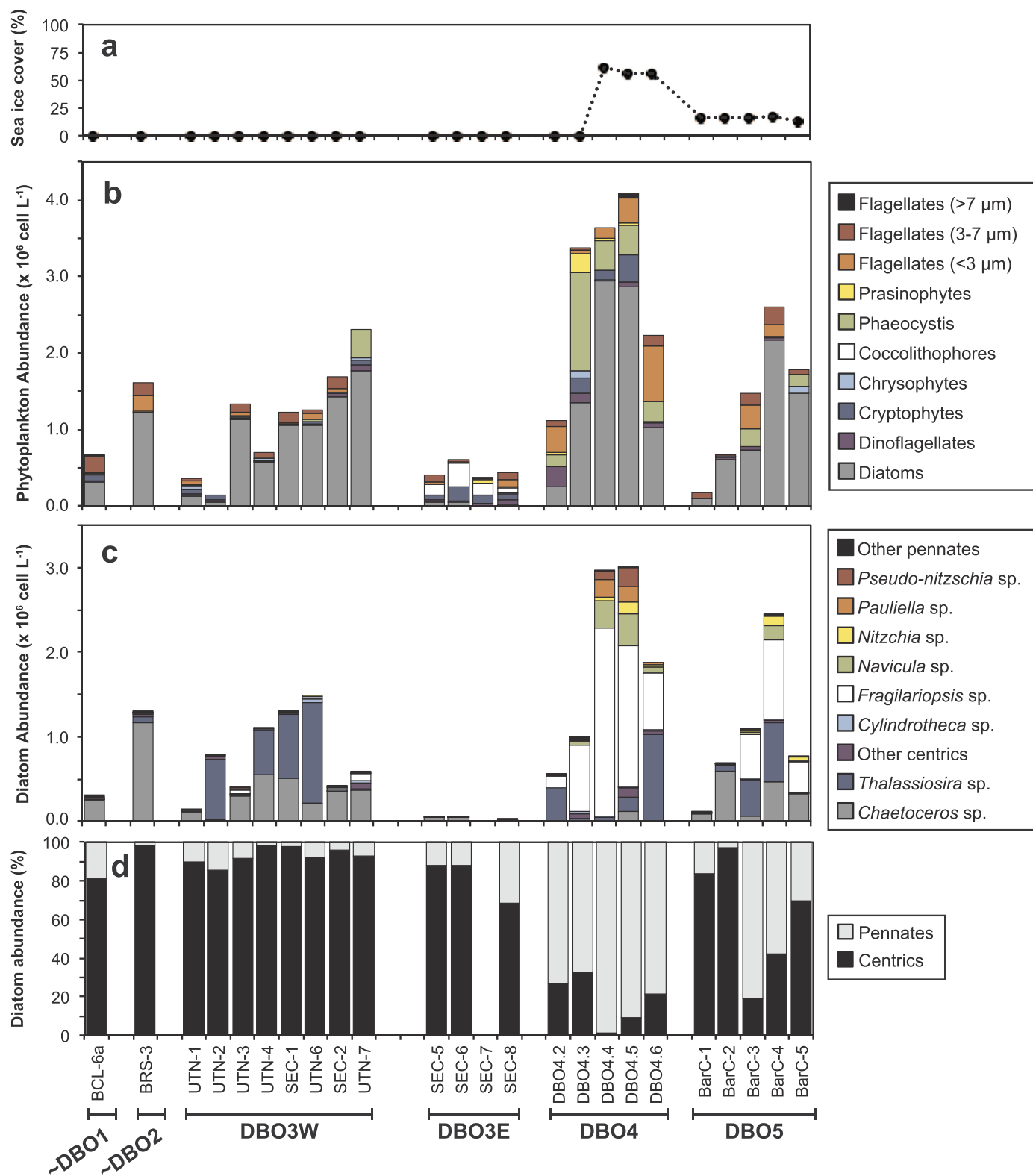
Fig. 6. Sea-ice concentration and phytoplankton assemblage composition for each station in July 2013. (a) Three-day mean of sea-ice concentration (%). (b) Cell abundance of major phytoplankton taxonomic groups. (c) Abundance of the prominent diatom taxa. (d) Relative abundance of centric versus pennate diatoms. Taxonomic data presented in panels b to d is derived from samples collected at the depth of the chlorophyll maximum (or at 5 m depth if maximum was not identified). The three size classes of flagellates (< 3 μm, 3–7 μm and > 7 μm) were undetermined species of likely different taxonomic affinities. Data from the DBO3 region are separated into west (DBO3W) and east (DBO3E) as in previous figures.

[NO$_3^-$] in surface waters. This result could be tied to the timing of the seasonal phytoplankton bloom and grazing by zooplankton. Campbell et al. (2009) found that grazing rates by mesozooplankton doubled in summer compared to spring in the Chukchi Sea, with mesozooplankton consuming ~28% of primary productivity per day in summer. A concurrent study by Sherr et al. (2009) indicated that grazing by

Table 5
Phytoplankton taxa present at 10 or more stations in the PAR in 2013. Data are summarized for the entire PAR and by DBO region. The total number of stations where phytoplankton taxonomic analysis was conducted within each region is listed in parentheses below the region.

Group	Taxa present at 10 or more stations	Number of stations where taxa present						
		Total (24)	DBO1 (1)	DBO2 (1)	DBO3W (8)	DBO3E (4)	DBO4 (5)	DBO5 (5)
Flagellates $< 7\,\mu m$	Flagellates $< 3\,\mu m$	19	1	1	6	4	3	5
	Flagellates $3–7\,\mu m$	20	1	1	6	4	5	2
Cryptomonads (Cryptophyceae)	*Cryptomonas* sp.	10	0	0	4	4	2	0
Prymnesiophyceae	*Phaeocystis pouchetii*[*]	11	0	0	3	1	5	2
Diatoms (Bacillariophyceae)	*Chaetoceros convolutus*	10	1	1	7	0	0	1
	Chaetoceros furcellatus spores	14	1	1	7	2	0	3
	Chaetoceros furcellatus	11	1	1	6	1	0	2
	Chaetoceros socialis	11	1	1	6	0	1	2
	Cylindrotheca closterium	23	1	1	8	3	5	5
	Fragilariopsis cylindrus	10	0	0	3	0	4	3
	Fragilariopsis oceanica	14	0	1	5	0	4	4
	Thalassiosira $> 30\,\mu m$	11	0	1	4	0	3	3
	Thalassiosira antarctica v. *borealis*	12	0	0	4	0	5	3
	Thalassiosira nordenskioeldii	14	0	1	5	0	4	4

[*] single cells.

microzooplankton can also be an important process limiting phytoplankton biomass during the later stages of a bloom. However, combined microzooplankton-mesozooplankton grazing was found to only consume a total of ~44% of primary productivity per day, which is still much lower than in other polar marine ecosystems such as the Barents Sea or the Southern Ocean (e.g. Table 4 in Sherr et al., 2009 and references therein).

Zooplankton may have also indirectly affected phytoplankton productivity in DBO2 through increased NH_4^+ release from excretion and nutrient regeneration into the water column (e.g Steinberg and Saba, 2008), which, in turn, could inhibit ρNO_3 by phytoplankton as indicated for DBO1 above. This grazing-associated increase in $[NH_4^+]$ could limit the accumulation of Chl *a* and drive the system into a steady-state based on the use of regenerated nitrogen. The range of $[NH_4^+]$ observed in DBO2 during our sampling time was similar to that in DBO1 (i.e. ~0.5 $\mu mol\,L^{-1}$ and 1–3 $\mu mol\,L^{-1}$ in the upper and lower euphotic zone, respectively; data from Cooper and Grebmeier, 2016a, 2016b, Cooper et al., 2016a, 2016d, 2016b, 2016c, 2017). In both DBO regions, $[NH_4^+]$ were higher than those observed earlier in the season (e.g. Lee et al., 2012), indicating that NH_4^+ accumulated in the water column through the growing season up to levels that could be inhibiting ρNO_3 for some phytoplankton. However, diatoms, which are the dominant phytoplankton taxon throughout the nutrient rich waters of the Pacific Arctic (Figs. 5 and 6), have higher half-inhibition constants for NO_3^- utilization by NH_4^+ (K_i = ~2.7 $\mu mol\,L^{-1}$ from Lomas and Glibert, 1999) compared to other phytoplankton (e.g. K_i = 0.24 $\mu mol\,L^{-1}$ for the coccolithophore *Emiliania huxleyi* from Varela and Harrison, 1999), meaning that diatom utilization of NO_3^- is inhibited at higher $[NH_4^+]$ compared to other phytoplankton. Furthermore, while $[NH_4^+]$ in the upper euphotic zone was below the K_i threshold for diatoms in both DBO1 and DBO2, $[NO_3^-]$ was much higher in the upper euphotic zone of DBO2 compared to DBO1, which may explain the higher productivity in DBO2 as there was simply more NO_3^- available to support phytoplankton growth.

The highest ρC and ρNO_3 in the PAR were generally found in the western sector of DBO3, likely the result of turbulent vertical mixing in the Chirikov Basin and Bering Strait providing nutrients to surface waters. Similar to $[NO_3^-]$ and Chl *a* distributions, east to west gradients in ρC and ρNO_3 were observed in DBO3, with the highest ρC and ρNO_3 in the western sector (station UTN-4), and lowest in the eastern sector (station SEC-5). Primary productivity and ρNO_3 continued to decrease northwards from DBO3 to DBO5 as $[NO_3^-]$ in surface waters decreased, likely a result of the intense productivity occurring in the southeastern Chukchi Sea (DBO3) and the lack of replenishment of nutrients as the waters travel north.

4.1.3. f-ratios and C export

The average *f*-ratio for all DBO regions was 0.41 $\pm$ 0.24, which agrees well with previous results (Table 6). Some spatial variability was observed among DBO regions, with *f*-ratios being higher closer to the shelf edges (DBO1, DBO4 and DBO5), although differences were not significant. The effect of water mass differences in DBO3 was also evident in *f*-ratios, which were higher in the western sector (0.37) than in the eastern sector (0.15), as also seen in previous studies (Hansell and Goering, 1990; Lee et al., 2007).

On an annual basis and assuming steady-state, New-Prod can be considered equivalent to the amount of C available for export or net community production (NCP) in most marine systems (e.g. Platt et al., 1989). However, due to the high interannual variability of the PAR and limited temporal sampling of our study, it is challenging to use our one-time, short-term measurements to make such estimates. New-Prod in the Bering and Chukchi Seas was calculated in previous studies from the seasonal drawdown of $[NO_3^-]$ (e.g. Sambrotto et al., 1984; Hansell et al., 1993), which may better reflect seasonal variations in primary productivity. Despite our New-Prod measurements only representing a snapshot of the growing season, our average daily New-Prod in the nutrient-rich waters of DBO3W (2.34 $\pm$ 0.78 $g\,C\,m^{-2}\,d^{-1}$; Table 3) is remarkably close to the estimate based on the seasonal $[NO_3^-]$ drawdown given by Hansell et al. (1993) for the same location (2.4 $g\,C\,m^{-2}$ d^{-1}). While this agreement may suggest that our results could be extended to longer temporal and spatial scales, our estimates of daily New-Prod in the regions south of the Bering Strait (0.48 $\pm$ 0.13 $g\,C$ $m^{-2}\,d^{-1}$ for DBO1–2; Table 3) were much lower than the value reported by Hansell et al. (1993) for the same area (3.1 $g\,C\,m^{-2}\,d^{-1}$). This difference between our estimate and that of Hansell et al. (1993) for DBO1–2 could reflect the timing of our sampling with respect to the peak of the seasonal bloom in these regions (e.g. Cooper et al., 2012), since a lower New Prod estimate would be expected under post-bloom conditions. However, this difference could also reflect a longer-term (yearly) decrease in productivity, which is consistent with previously documented declines in primary productivity (Lee et al., 2012) and benthic biomass (Grebmeier et al., 2006b) in the region. Nevertheless, these comparisons highlight the importance of accounting for time and seasonal scales when attempting to equate New-Prod (estimated from short-term measurements of ρNO_3) to annual C export.

4.1.4. Phytoplankton assemblages

The Bering and Chukchi Seas are dominated by diatoms, as shown by our 2013 phytoplankton composition data and previous studies (e.g. Gosselin et al., 1997; Booth and Horner, 1997; Hill and Cota, 2005; Sukhanova et al., 2009; Poulin et al., 2010; Coupel et al., 2012; Joo

Table 6

Depth-integrated primary productivity (ρC), nitrate utilization rates (ρNO_3) and *f*-ratios (mean ± SE) within or near the five DBO hotspot regions in the Bering and Chukchi Seas for June-August from 1954 to 2016. Data from DBO3 is split longitudinally into the western (DBO3W, influenced by the AW/BSW water mass) and eastern (DBO3E, influenced by the ACW water mass) sectors. Bold indicates data from this study and (-) indicates that no data are available. The number in parenthesis after the standard error (SE) indicates the number of samples. ICESCAPE stands for the 'Impacts of Climate on the Eco-Systems and Chemistry of the Arctic Pacific Environment' project.

Region	Date (Month, Year)	ρC (g C m^{-2} d^{-1})	ρNO_3 (mmol N m^{-2} d^{-1})	*f*-ratio	Data source
Northern Bering Shelf					
DBO1	**Jul 2006–2016**	**0.34 ± 0.08 (8)**	**6.30 ± 1.64 (8)**	**0.53 ± 0.09 (3)**	This study and Varela et al. (2013)
	Aug 1988	3.8 ± (-)	–	–	Springer and McRoy (1993)
	May-Jun 2007	0.99 ± 0.23 (12)	7.81 ± 1.28 (12)	0.76 ± 0.03 (12)	Lee et al. (2012)
	Jul 2007	0.17 ± 0.07 (2)	5.31 ± 3.36 (15)[a]	0.43 ± 0.16 (3)	Lee et al. (2013a)
DBO2	**Jul 2006–2016**	**1.00 ± 0.34 (8)**	**7.19 ± 3.53 (8)**	**0.37 ± 0.11 (7)**	This study and Varela et al. (2013)
	Jun-Sep 1969–1983	2.7 ± (-)	17.6 ± (-)	0.55 ± (n.d.)	Sambrotto et al. (1984)
	Jul-Sep 1987	–	8.0 ± 0.7 (15)	0.30 ± (n.d.)	Hansell and Goering (1990)
	Aug 1988	4.0 ± (-)	–	–	Springer and McRoy (1993)
	May-Jun 2007	1.03 ± 0.04 (3)	11.1 ± 3.2 (3)	0.83 ± 0.05 (3)	Lee et al. (2012)
Entire region (DBO1-DBO2)					
	Jul 2006–2016	**0.67 ± 0.19 (16)**	**6.74 ± 1.88 (16)**	**0.42 ± 0.08 (10)**	This study and Varela et al. (2013)
	Jul 1950–2012	1.8 ± 0.26 (68)	–	–	Hill et al. (2017)
	May-Sep 1954–2007	–	8.41 ± (-)[c]	0.4	Codispoti et al. (2013)
Southeastern Chukchi Sea					
DBO3W	**Jul 2006–2016**	**3.40 ± 1.01 (7)**	**29.7 ± 12.0 (7)**	**0.48 ± 0.10 (6)**	This study and Varela et al. (2013)
	Jul-Sep 1987	–	45.6 ± 0.7(2)[b]	0.50 ± (n.d.)	Hansell and Goering (1990)
	Jun-Aug 2002–2004	1.44 ± 0.66 (5)	10.0 ± 4.6 (5)[b]	0.41 ± 0.20 (5)	Lee et al. (2007)
DBO3E	**Jul 2006–2016**	**0.15 ± 0.08 (2)**	**0.31 ± 0.23 (2)**	**0.16 ± 0.08 (2)**	This study and Varela et al. (2013)
	Jul-Sep 1987	–	2.30 ± 0.54 (3)[b]	0.15 ± (-)	Hansell and Goering (1990)
	Jun-Aug 2002–2004	0.14 ± 0.04 (2)	1.02 ± 0.25 (2)[b]	0.19 ± 0.09 (2)	Lee et al. (2007)
Entire region (DBO3, all water masses)					
	Jul 2006–2016	2.68 ± 0.91 (9)	23.2 ± 10.2 (9)	0.40 ± 0.09 (9)	This study and Varela et al. (2013)
	Jul 1950–2012	3.02 ± 0.18 (22)	–	–	Hill et al. (2017)
	May-Sep 1954–2007	–	10.3 ± (n.d.)[c,d]	0.3[d]	Codispoti et al. (2013)
	Jul 1974	1.3 ± 1.1 (3)	–	–	Hameedi (1978)
	Aug 1988	4.7 ± (-)	–	–	Springer and McRoy (1993)
	Jun-Aug 2002–2004	1.07 ± 0.56 (7)	8.22 ± 4.16 (7)[b]	0.35 ± 0.18 (7)	Lee et al. (2007)
	Aug 2007	1.61 ± 0.56 (4)	5.31 ± 3.36 (15)[a]	0.72 ± 0.11 (2)	Lee et al. (2013a)
	Jun 2010–2011	12.90 ± 3.25 (2)	–	–	Arrigo ICESCAPE unpubl. data (from Grebmeier et al. (2015))
Northeastern Chukchi Sea					
DBO4	**Jul 2006–2016**	**1.17 ± 0.39 (6)**	**8.84 ± 4.13 (6)**	**0.41 ± 0.12 (5)**	This study and Varela et al. (2013)
	Jul 1974	1.3 ± 1.0 (3)	–	–	Hameedi (1978)
	Aug 1993	0.49 ± 0.17 (3)	1.11 ± 0.48 (3)[e]	0.17 ± 0.12 (3)	Cota et al. (1996)
	Jul-Aug 2002/2004	0.67 ± 0.06 (2)	–	–	Hill and Cota (2005)
	Aug 2007	0.18 ± 0.03 (6)	5.31 ± 3.36 (15)[a]	–	Lee et al. (2013a)
	Jul 2010–2011	0.67 ± 0.06 (2)	–	–	Arrigo ICESCAPE unpubl. data (from Grebmeier et al. (2015))
DBO5	**July 2008/2015**	**0.99 ± 0.59 (2)**	**8.55 ± 2.55 (2)**	**0.50 (1)**	This study and Varela et al. (2013)
	Jul 2002	~2	–	–	Hill and Cota (2005)
Entire region (DBO4-DBO5)					
	Jul 2006–2016	**1.13 ± 0.33 (8)**	**8.77 ± 3.31 (8)**	**0.43 ± 0.12 (6)**	This study and Varela et al. (2013)
	Jul 1950–2012	2.02 ± 0.47 (33)	–	–	Hill et al. (2017)
	May-Sep 1954–2007	–	5.89 ± (-)[c,d]	0.3[e]	Codispoti et al. (2013)
	Aug 2008	1.38 ± 0.49 (11)	–	–	Coupel et al. (2015)

[a] Average rates for Northern Bering Sea to Northern Chukchi Sea.

[b] Average daily rates were calculated from hourly rates assuming a 15-h photoperiod (Hansell and Goering, 1990).

[c] Average daily rates were calculated from annual net community production (NCP), derived from *in situ* changes in [NO$_3^-$] and [PO$_4^{3-}$], assuming an 86-day productive season and a C:N ratio of 6.6 (Tables 3, 5 in Codispoti et al., 2013).

[d] Southern Chukchi Sea from Codispoti et al. (2013) covers DBO3-5.

[e] Average daily rates were calculated from daily primary production (based on ^{13}C utilization rates) and % new production based on ^{15}NO$_3^-$ utilization rates and assuming a C:N ratio of 6.6 (Cota et al., 1996, Table 2).

et al., 2012; Lee et al., 2012; Wyatt et al., 2013; Crawford et al., 2018). Diatoms accounted for 65 ± 21% of the total phytoplankton assemblage, on average, for all DBO regions, with the exception of four stations in the eastern sector of DBO3 (SEC-5 to SEC-8). In DBO3E, the assemblage was primarily composed of coccolithophores and small (< 7 μm) unidentified flagellates. The presence of small non-diatom phytoplankton can be explained by the differences in water mass composition and lower nutrient content in the eastern sector of DBO3 in comparison to the western sector (see Section 4.2.2). Diatom abundance increased slightly towards the north (Fig. 6b), likely due to the timing of the seasonal retreat of sea-ice and the northward propagation of the seasonal bloom (i.e. earlier stages of a bloom would be expected to have a larger diatom presence). In DBO4, an increase in the

abundance of pennate diatoms (primarily *Fragilariopsis* spp.) was associated with the presence of sea-ice. It is possible that the increased abundance of this diatom in the water column was due to sea-ice algae being released from sea-ice algal blooms, given that *Fragilariopsis* spp. are commonly found in sea ice (e.g. Booth and Horner, 1997; Lundholm and Hasle, 2010). However, our 2013 observations of very high ρC and ρNO_3 at 7–10 m depth combined with extremely low [NO$_3^-$] in the euphotic zone (range: 0 – 0.7 μmol L^{-1}) in DBO4 are indicative of an actively growing phytoplankton community below the ice. Several studies have reported the existence of diatom blooms near or below the ice in the Chukchi Sea (e.g. Booth and Horner, 1997; Coupel et al., 2012; Arrigo et al., 2014), although typically the assemblage composition is dominated by centric diatoms, such as *Chaetoceros* spp. and

Thalassiosira spp., that are generally associated with the late stage of a pelagic bloom. Arrigo et al. (2014) also found *Fragilariopsis* species in an under-ice bloom and argued that these were pelagic species and not the remnant of a sea-ice bloom. Similar to Arrigo et al. (2014), we cannot rule out that the diatoms present in the under-ice bloom were seeded from the sea-ice, even if our results suggest that they were part of a pelagic bloom.

Similar to diatoms, small (< 7 μm) flagellates were also present in all of the DBO regions during 2013, and slightly increased in abundance northwards. These flagellates were shown to dominate the phytoplankton assemblages in the oligotrophic waters of the Canada Basin (Crawford et al., 2018), but were also present on the Chukchi Shelf (e.g. Gosselin et al., 1997; Coupel et al., 2012; Crawford et al., 2018). Small flagellate plankton < 7 μm are usually present throughout the global oceans under a variety of nutrient and light conditions (e.g. Chisholm, 1992); however, they typically only dominate the assemblage composition under low nutrient concentrations, which are less favourable to the growth of other phytoplankton (e.g. Pasciak and Gavis, 1974; Chisholm, 1992). Single cells of the small, flagellated species *Phaeocystis pouchetii* were present in the Chukchi Sea and were most abundant in DBO4, where total phytoplankton abundance was high. This species is often observed after the late stages of the seasonal bloom in polar waters (e.g. Sakshaug, 2004), or co-occurring with diatoms (e.g. Wassmann et al., 1999; Olli et al., 2002), and can be a significant contributor to the vertical flux of C (Smith et al., 1991). The presence or absence of *Phaeocystis pouchetii* colonies can serve as an indicator of the stage of a phytoplankton bloom, with colonies disappearing toward the late stages of a bloom (e.g. Estep et al., 1990). The high abundance of both diatoms and single cells of *Phaeocystis pouchetii* in DBO4, but the lack of colonies of *Phaeocystis pouchetii*, suggest that our sampling may have occurred after the peak of the seasonal phytoplankton bloom.

Size fractionated measurements of Chl *a* are a relatively simple way to assess the size structure of phytoplankton assemblages. While no taxonomic data can be obtained from these measurements, this information is still important especially given that different size classes tend to dominate under different environmental conditions (Chisholm, 1992) and that zooplankton grazing rates depend on the phytoplankton size structure (Żurek and Bucka, 1994). The average contribution of the > 5 μm Chl *a* to total Chl *a* for all productivity stations in 2013 was 77 ± 13% (± SD), and for the entire study period (2006–2016) it was 65 ± 23%. Neither of these values are significantly different from the percent contribution of diatoms to total cell numbers in 2013, which suggests that the > 5 μm Chl *a* size fraction could be used as a proxy for diatom biomass in this region. Furthermore, Wyatt et al. (2013) found a significant positive correlation between diatom abundance and the contribution of the > 5 μm Chl *a* size fraction in marine waters throughout the Arctic. Thus, while the taxonomy of phytoplankton assemblages is only presented for 2013, size-fractionated Chl *a* data show evidence of spatial and interannual differences in the structure of phytoplankton assemblages between the Bering Sea (DBO1 and DBO2) and the Chukchi Sea (DBO3 to DBO5) during the 10-year period (Table 3; Fig. 3c).

4.2. Drivers of regional differences in phytoplankton biomass and productivity in the Pacific Arctic Region

4.2.1. Environmental controls

The correlation analysis between euphotic-zone integrated biological parameters and several physical parameters indicated that there were geographical differences in bottom-up controls on phytoplankton biomass and productivity between the Bering Sea (DBO1, DBO2) and Chukchi Sea regions (DBO3-DBO5) (Table 4).

In the Bering Sea, [NO_3^-] was positively correlated with surface and bottom S, which likely reflects the influence of the saline and nutrient-rich AW. The negative correlation between Z_{eu} and bottom T could be the result of earlier sea-ice retreat from 2012 to 2016 causing increased

water column stratification and an earlier shift in the seasonal bloom (Grebmeier et al., 2018; Frey et al., this issue). Bottom water temperatures in DBO1 are relatively low in summer, experiencing only limited warming from their winter values as a result of persistent water column stratification (e.g. Cooper et al., 2012; Grebmeier et al., 2015). Earlier sea-ice melt could result in an even greater degree of stratification due to low-salinity surface waters having move time to warm, thus further limiting mixing of the water column and resulting in bottom water temperatures even closer to their very low winter values (Cooper et al., 2012). Earlier sea-ice retreat also results in an earlier onset of the seasonal bloom (Brown et al., 2013), meaning that by the time of our sampling each year, we are sampling later and later into the seasonal bloom, resulting in changes in phytoplankton phenology from year-to-year (see Section 4.2.3). Changes in the abundance and type of phytoplankton present in the euphotic zone could allow light to penetrate deeper into the water column, and thus for the euphotic zone depth to increase. The positive correlations between ρC and both ρNO_3 and New-Prod indicate that NO_3^- was responsible for the high rates of primary production in the Bering Sea. Furthermore, the positive correlation between Chl *a* > 5 μm and New-Prod indicates that larger phytoplankton were the primary drivers of new production. The lack of a correlation between ρNO_3 and [NO_3^-] may indicate that phytoplankton were not limited by the availability of NO_3^- in the Bering Sea. This is consistent with results from Lee et al. (2013a), who found that light, rather than NO_3^-, had a larger influence on ρC in marine Arctic regions. In addition to light, our study suggests that bloom timing and zooplankton grazing could also influence rates of primary productivity in July (see Section 4.1.2).

In the Chukchi Sea, no significant correlations were found between biological and physical water-column parameters, but it is highly unlikely that there were no physical controls on primary productivity during July. Alternatively, it is possible that other parameters, not considered in this study, may have affected productivity more strongly during this period. The lack of significant correlations may have also resulted from high interannual variability in the T-S properties of the different water masses (e.g. Coachman, 1975; Woodgate et al., 2005b), which could have confounded the correlations if the drivers of the physical variability did affect the biology in a similar way. Our statistical analyses suggest that phytoplankton > 5 μm were the major contributors to total Chl *a* and primary productivity in the Chukchi Sea. Contrary to the situation in the Bering Sea, ρNO_3 and [NO_3^-] were positively correlated in the Chukchi Sea, potentially due to a broader range of values for ρNO_3 and [NO_3^-] strengthening the correlations. This result indicates that [NO_3^-] exerted a stronger control on productivity towards the northern regions of DBO during July.

In summary, our correlation analysis indicates that phytoplankton were not limited by NO_3^- availability on the Northern Bering Sea and that NO_3^- utilization by phytoplankton > 5 μm in size (primarily diatoms) drove the high rates of primary productivity throughout both the Northern Bering Sea and Chukchi Sea. This analysis also suggests that light, bloom timing, and zooplankton grazing could have a significant influence on primary productivity during July.

4.2.2. Water mass effects on phytoplankton assemblage composition and productivity

In 2013, a direct east-west comparison of the phytoplankton assemblage composition was conducted at all CTD/rosette stations in the southern Chukchi Sea. A similar direct comparison of euphotic zone [NO_3^-], Chl *a*, ρC and ρNO_3 was conducted at the productivity stations UTN-4 (DBO3W) and SEC-5 (DBO3E) in 2014. A strong east-west gradient in [NO_3^-], and phytoplankton biomass, productivity and assemblage composition was found in the DBO3 region (Figs. 2–6, Table 3). The values of these biological parameters were up to two orders of magnitude lower on DBO3E compared to DBO3W, and these differences coincided with changes in T, S and [NO_3^-] measured at all CTD/rosette stations in DBO3 (Fig. 7; data from Cooper et al., 2016b). The T, S, and
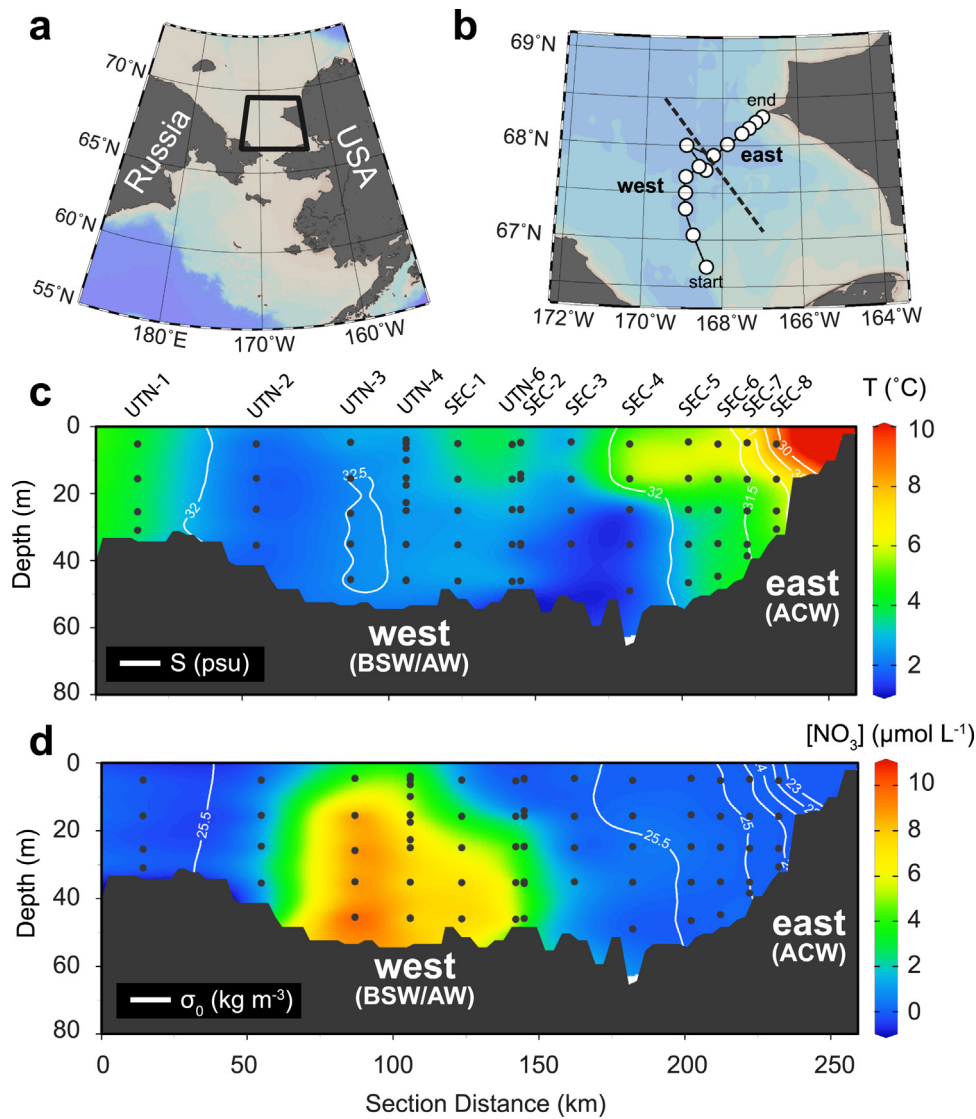
Fig. 7. Physico-chemical differences between the Alaska Coastal Water (ACW) in the east and Bering Shelf Water (BSW/AW) in the west, along the DBO3 transect in the southeastern Chukchi Sea in July 2013. (a) Map of the PAR, with the black box denoting the bounding coordinates for panel b. (b) Map of the transect line. (c) Vertical section of temperature (T) with contours of salinity (S) superimposed in white. (d) Vertical section of NO_3^- concentration with contours of potential density (σ_0) superimposed in white. T-S data for all stations, and $[NO_3^-]$ data from CTD/rosette stations are from Cooper et al. (2016b).

$[NO_3^-]$ data we present in Fig. 7 are only for 2013 so that spatial trends in these parameters are directly comparable with the phytoplankton assemblage data shown in Fig. 6; however, similar spatial differences between W and E for T, S and $[NO_3^-]$ were observed during other years, including 2014 (Figs. 2-3, Table 3; Cooper and Grebmeier, 2016a, 2016b; Cooper et al., 2016a, 2016d, 2016b, 2016c, 2017). Abundant phytoplankton assemblages in DBO3W were dominated by diatoms, in contrast to the flagellate- and coccolithophore-dominated assemblages of DBO3E. Previous studies in nearby areas of the northern Bering and Chukchi Seas have also shown an east-west gradient in nutrients, Chl a and the size structure of phytoplankton assemblages (e.g. Walsh et al., 1989; Cooper et al., 2012; Danielson et al., 2017), and primary productivity (Lee et al., 2007), likely driven by the presence of different waters masses on each side of the transect.

The nutrient poor waters of ACW on DBO3E cannot support the high rates of primary production and high diatom abundance characteristic of DBO3W and the other DBO regions. In contrast, coccolithophores and other small phytoplankton are better adapted to the low nutrient conditions of DBO3E given their higher surface area to volume ratios and typically lower nutrient half-saturation constants (K_s) than diatoms

(e.g. Eppley et al., 1974). The presence of coccolithophores in the PAR is not unprecedented (e.g. Napp and Hunt, 2001; Stockwell et al., 2001). A sustained bloom that lasted > 2–3 months was first observed in the Bering Sea in 1996 using satellite ocean color (Merico et al., 2003); however, there has been some indication that coccolithophore abundance in the Bering Sea has decreased in recent years (Iida et al., 2012) due to reduced surface stratification.

Although DBO focuses on biological hotspots, the east-west gradient observed in DBO3 suggests that large spatial variability in water-column physical, chemical and biological parameters could still exist within each of the DBO regions. Furthermore, these spatial variations in water mass composition and properties coincide with changes in benthic ecosystems in DBO3 (e.g. Grebmeier et al., 2015). Given that diatoms are the major contributor to phytoplankton biomass and productivity in the nutrient-rich waters that overlay benthic hotspots, it is important to consider how climate-induced changes can impact diatom dynamics and how this may cascade up the food web and affect pelagic-benthic coupling. Increasing temperatures and changing sea-ice cover may result in summertime conditions that are unfavourable to diatoms, but instead support the growth of coccolithophores and other small

phytoplankton, as seen in the oligotrophic Arctic basin (Li et al., 2009) and in DBO3E (this study). Climatic changes throughout the PAR could also lead to variations in plankton phenology, including a shorter period of sea-ice algal production and a longer period of pelagic production. Changes in phenology could ultimately result in a shift from benthic to pelagic-dominated marine ecosystems (e.g. Grebmeier et al., 2006a, 2006b; Moore and Stabeno, 2015). These effects could be further exacerbated if the contribution of nutrient-rich AW to the Chukchi Sea decreased, or if there were changes to the T-S properties of waters flowing through the Bering Strait. Previous studies documented decreases in the volume and distribution of AW into the region that contributed to significant decreases in primary productivity and the contribution of larger ($> 5\,\mu m$) cells to the phytoplankton assemblage (Lee et al., 2013b; Yun et al., 2014). However, these biological changes could have also been driven by variations in phytoplankton phenology due to increased temperatures and decreased salinities of the Bering Strait inflow (Woodgate, 2018). Ultimately, a negative impact to the base of the regional food web could result in the loss of the DBO benthic hotspots and, furthermore, they could have far reaching consequences for biogeochemical fluxes and climate feedbacks in the region and further into the Arctic.

4.2.3. Temporal trends and interannual variability in the Bering and Chukchi Seas

We compared historical measurements of phytoplankton productivity with our own findings for the five DBO regions (Table 6). While there is fairly good agreement between this and past studies, it is unclear whether any differences are indicative of year-to-year productivity changes in the region, or simply the result of differences in the time of sampling (i.e. earlier vs. later in the growing season), in methodology (i.e. productivity method, incubation time), in sampling location, and, most importantly, whether the changes are due to the lack of comprehensive spatial and temporal coverage. Therefore, it is difficult to draw any significant conclusions regarding changes prior to 2006.

Our sampling occurred at the same time (mid-July) and used consistent methodology every year from 2006 to 2016 to allow for valid comparisons. We observed large interannual variations in all parameters, with almost no consistent year-to-year trends throughout the 10-yr period (i.e. see Table 3 and Figs. 4–6). These results exemplify the difficulties in identifying long-term trends in this region. One exception was a significant decreasing trend in the contribution of the $> 5\,\mu m$ Chl *a* to total Chl *a* in DBO1 from 2012 to 2016. This trend could have been the result of a shift in the timing of the spring bloom from later to earlier in the growing season, meaning that with each passing year we sampled later stages of the phytoplankton spring bloom. Brown and Arrigo (2013) showed that the timing of the spring bloom on the Bering Sea shelf was dependant on the timing of the seasonal sea-ice breakup. Although decadal changes in the mean timing of sea-ice breakup were not observed in DBO1 from 1978 to 2012 (Grebmeier et al., 2015), this timing did decrease over the shorter 2012–2016 period (Grebmeier et al., 2018; Frey et al., this issue), which suggests that spring blooms could have happened earlier with the passing years from 2012 to 2016. While the decrease in the proportion of $> 5\,\mu m$ Chl *a* over this period indicates that phytoplankton phenology responds to short-term environmental changes, it is difficult to know whether or not such changes to the ecosystem can be sustained throughout a longer period given the naturally high interannual variability of the region. These results further highlight the need for long-term and consistent monitoring programs, like DBO, to better understand present and future climate-induced changes on the productive ecosystems of the PAR.

5. Conclusions

We present here a decade of information on phytoplankton and nutrient dynamics during summer for five biological 'hotspots' in the northern Bering and Chukchi Seas. Although interannual variability was high for all measured parameters, we consistently found that diatoms dominated the phytoplankton assemblages throughout most of the DBO regions, and phytoplankton biomass and productivity were high under the influence of the nutrient rich AW. In contrast, the coastal region of the southeastern Chukchi Sea was dominated by coccolithophores and flagellated plankton and characterized by low euphotic zone [NO$_3^-$], and low phytoplankton biomass and productivity. These contrasting results demonstrate the presence of an east to west gradient in phytoplankton assemblage composition, biomass, and productivity in the southeastern Chukchi Sea that could be attributed to differences in the nutrient content of the water masses affecting these locations. Another highlight of this study is the finding that the presence or absence of sea-ice can impact the composition of phytoplankton assemblages. In the northern Chukchi Sea, pennate diatoms have higher abundances than centric diatoms when sea-ice was present. The low [NO$_3^-$], but high ρC and ρNO$_3$ throughout the euphotic zone of this northern region suggest that the abundance of pennate diatoms is the result of a pelagic boom rather than them being supplied by a sea-ice bloom. Finally, our results suggest that, because of the generally high [NO$_3^-$] within the euphotic zone throughout most DBO regions, light and/or grazing may exert a greater control on phytoplankton productivity than [NO$_3^-$] during July.

An important aspect of this work was the consistency in methodologies, and sampling time and locations throughout the 10 years that allowed for rigorous comparisons both temporally and spatially. Results from this study emphasize the significant interannual variability in phytoplankton biomass and productivity that cannot be attributed to differences in methodology. However, the highly dynamic nature of the PAR may be responsible for such large interannual variations and can complicate the identification of long-term trends.

This study contributes to our knowledge of temporal and spatial variations in summertime productivity for this region, but also illustrates the need for a better understanding of the long-term temporal variability that will likely only be revealed by increased sampling resolution, both seasonally and annually. The PAR is an important gateway for nutrients and biomass to the Arctic Ocean. Improving our ability to constrain climate-induced changes against the backdrop of natural interannual variability will greatly enhance our ability to predict how future environmental change will affect this ecologically and economically important region.

References

Arrigo, K.R., Perovich, D.K., Pickart, R.S., Brown, Z.W., van Dijken, G.L., Lowry, K.E., Mills, M.M., Palmer, M.A., Balch, W.M., Bates, N.R., Benitez-Nelson, C.R., Brownlee, E., Frey, K.E., Laney, S.R., Mathis, J., Matsuoka, A., Mitchell, B.G., Moore, G.W.K., Reynolds, R.A., Sosik, H.M., Swift, J.H., 2014. Phytoplankton blooms beneath the sea ice in the Chukchi sea. Deep-Sea Res. II 105, 1–16. https://doi.org/10.1016/j.dsr2.2014.03.018.

Barwell-Clarke, J., Whitney, F.A., 1996. Institute of Ocean Sciences nutrient methods and analysis. Can. Tech. Rep. Hydrogr. Ocean Sci. 182, 1–49.

Beardall, J., Morris, I., 1976. The concept of light intensity adaptation in marine phytoplankton: some experiments with Phaeodactylum tricornutum. Mar. Biol. 37, 377–387.

Booth, B.C., Horner, R.A., 1997. Microalgae on the Arctic Ocean Section, 1994: species abundance and biomass. Deep-Sea Res. II 44, 1607–1622.

Brown, Z.W., Arrigo, K.R., 2013. Sea ice impacts on spring bloom dynamics and net primary production in the Eastern Bering Sea. J. Geophys. Res. Oceans 118, 43–62. https://doi.org/10.1029/2012JC008034.

Brown, Z.W., Lowry, K.E., Palmer, M.A., van Dijken, G.L., Mills, M.M., Pickart, R.S., Arrigo, K.R., 2015. Deep-Sea Res. II. Deep-Sea Res. II 118, 88–104. https://doi.org/10.1016/j.dsr2.2015.02.010.

Brown, Z.W., van Dijken, G.L., Arrigo, K.R., 2011. A reassessment of primary production and environmental change in the Bering Sea. J. Geophys. Res. 116, 1111. https://doi.org/10.1029/2010JC006766.

Campbell, R.G., Sherr, E.B., Ashjian, C.J., Plourde, S., Sherr, B.F., Hill, V., Stockwell, D.A., 2009. Mesozooplankton prey preference and grazing impact in the western Arctic Ocean. Deep-Sea Res. II 56, 1274–1289. https://doi.org/10.1016/j.dsr2.2008.10.027.

Carmack, E., Wassmann, P., 2006. Food webs and physical–biological coupling on pan-Arctic shelves: unifying concepts and comprehensive perspectives. Progress. Oceanogr. 71, 446–477.

Cavalieri, D.J., Parkinson, C.L., 2012. Arctic sea ice variability and trends, 1979–2010. Cryosphere 6, 881–889. https://doi.org/10.5194/tc-6-881-2012.

Chisholm, S.W., 1992. Phytoplankton Size. In: Falkowski, P.G., Woodhead, A.D., Vivirito, K. (Eds.), Primary Productivity and Biogeochemical Cycles in the Sea, Primary Productivity and Biogeochemical Cycles in the Sea. Springer, US, Boston, MA, pp. 213–237.

Coachman, L.K., Aagaard, K., 1966. On the Water Exchange Through Bering Strait. Limnol. Oceanogr. 11, 44–59. https://doi.org/10.4319/lo.1966.11.1.0044.

Coachman, L.K., Aagaard, K., Tripp, R.B., 1975. Bering Strait: the regional physical oceanography. University of Washington Press.

Codispoti, L.A., Kelly, V., Thessen, A., Matrai, P., Suttles, S., Hill, V., Steele, M., Light, B., 2013. Synthesis of primary production in the Arctic Ocean: iii. Nitrate and phosphate based estimates of net community production. Progress. Oceanogr. 1–25. https://doi.org/10.1016/j.pocean.2012.11.006.

Cooper, L.W., Janout, M.A., Frey, K.E., Pirtle-Levy, R., Guarinello, M.L., Grebmeier, J.M., Lovvorn, J.R., 2012. The relationship between sea ice break-up, water mass variation, chlorophyll biomass, and sedimentation in the northern Bering Sea. Deep-Sea Res. II 65–70, 141–162. https://doi.org/10.1016/j.dsr2.2012.02.002.

Cooper, L.W., Grebmeier, J.M., 2016a. Sir Wilfrid Laurier (SWL) Cruise Merged Chemistry Parameters (2006). Arct. Data Cent. https://doi.org/10.5065/D6C24TGR.

Cooper, L.W., Grebmeier, J.M., 2016b. Sir Wilfrid Laurier (SWL) Cruise Merged Chemistry Parameters (2008). Arct. Data Cent. https://doi.org/10.5065/D6FT8J2S.

Cooper, L.W., Grebmeier, J.M., Vagle, S., 2016a. SWL11 Bottle data. Arct. Data Cent. https://doi.org/10.5065/D6F47M5P.

Cooper, L.W., Grebmeier, J.M., Vagle, S., 2016d. SWL12 Bottle data. Arctic Data Center. urn:uuid:a8194ad0-edb5-47bd-8fa1-33c24ed986d7.

Cooper, L.W., Grebmeier, J.M., Frey, K.E., Vagle, S., 2016b. SWL13 Bottle data. SWL13 Bottle data. Arct. Data Cent. https://doi.org/10.5065/D6VD6WHK.

Cooper, L.W., Grebmeier, J.M., Frey, K.E., Vagle, S., 2016c. SWL14 Bottle data. Arct. Data Cent. https://doi.org/10.5065/D6416V3G. (version: urn:uuid:26786355-86f3-4554-8e68-a5b668fd2698).

Cooper, L.W., Grebmeier, J.M., Frey, K.E., Vagle, S., 2016d. Sir Wilfrid Laurier (SWL) Bottle data 2015. Arct. Data Cent. https://doi.org/10.5065/D6QN6544. (version: urn:uuid:8400608d-cecd-4b48-a446-4dacf4b43435).

Cooper, L.W., Grebmeier, J.M., Frey, K.E., Vagle, S., 2017. Discrete water samples collected from the Conductivity-Temperature-Depth rosette at specific depths, Northern Bering Sea to Chukchi Sea, 2016. Arct. Data Cent. https://doi.org/10.18739/A22V25.

Cota, G.F., Pomeroy, L.R., Harrison, W., Jones, E.P., Peters, F., Sheldon, W.M., Weingartner, T.R., 1996. Nutrients, primary production and microbial heterotrophy in the southeastern Chukchi Sea: arctic summer nutrient depletion and heterotrophy. Mar. Ecol. Prog. Ser. 135, 247–258.

Coupel, P., Jin, H.Y., Joo, M., Horner, R., Bouvet, H.A., Sicre, M.A., Gascard, J.C., Chen, J.F., Garcon, V., Ruiz-Pino, D., 2012. Phytoplankton distribution in unusually low sea ice cover over the Pacific Arctic. Biogeosciences 9, 4835–4850. https://doi.org/10.5194/bg-9-4835-2012-supplement.

Coupel, P., Ruiz-Pino, D., Sicre, M.A., Chen, J.F., Lee, S.H., Schiffrine, N., Li, H.L., Gascard, J.C., 2015. Prog. Oceanogr. 131, 113–125. https://doi.org/10.1016/j.pocean.2014.12.003.

Crawford, D.W., Cefarelli, A.O., Wrohan, I.A., Wyatt, S.N., Varela, D.E., 2018. Progress in oceanography. Progress. Oceanogr. 162, 132–159. https://doi.org/10.1016/j.pocean.2018.01.006.

Danielson, S.L., Eisner, L., Ladd, C., Mordy, C., Sousa, L., Weingartner, T.J., 2017. A comparison between late summer 2012 and 2013 water masses, macronutrients, and phytoplankton standing crops in the northern Bering and Chukchi Seas. Deep-Sea Res. II 135, 7–26. https://doi.org/10.1016/j.dsr2.2016.05.024.

Danielson, S.L., Weingartner, T.J., Hedstrom, K.S., Aagaard, K., Woodgate, R.A., Curchitser, E., Stabeno, P.J., 2014. Coupled wind-forced controls of the Bering–Chukchi shelf circulation and the Bering Strait throughflow: ekman transport, continental shelf waves, and variations of the Pacific–Arctic sea surface height gradient. Progress. Oceanogr. 125, 40–61. https://doi.org/10.1016/j.pocean.2014.04.006.

Dickson, A., Goyet, C., 1994. Handbook of Methods for the Analysis of the Various Parameters of the Carbon Dioxide System in Sea Water. U. S. Dep. Energy.

Divoky, G.J., Lukacs, P.M., Druckenmiller, M.L., 2015. Effects of recent decreases in arctic sea ice on an ice-associated marine bird. Progress. Oceanogr. 136, 151–161. https://doi.org/10.1016/j.pocean.2015.05.010.

Dortch, Q., 1990. The interaction between ammonium and nitrate uptake in phytoplankton. Mar. Ecol. Prog. Ser. 183–201.

Duarte, C.M., Lenton, T.M., Wadhams, P., Wassmann, P., 2012. Abrupt climate change in the Arctic. Nat. Clim. Change 2, 60–62. https://doi.org/10.1038/nclimate1386.

Dugdale, R.C., Goering, J.J., 1967. Uptake of New and Regenerated Forms of Nitrogen in Primary Productivity. Limnol. Oceanogr. 12, 196–206.

Dugdale, R.C., Wilkerson, F.P., 1986. The use of 15N to measure nitrogen uptake in eutrophic oceans; experimental considerations. Limnol. Oceanogr. 31, 673–689.

Eppley, R.W., Rogers, J.N., McCarthy, J.J., 1974. Half-saturation constants for uptake of nitrate and ammonium by marine phytoplankton. Limnol. Oceanogr. 14, 912–920. https://doi.org/10.4319/lo.1969.14.6.0912.

Eppley, R.W., Peterson, B.J., 1979. Particulate organic matter flux and planktonic new production in the deep ocean. Nature 282, 677–680.

Estep, K.W., Nejstgaard, J.C., Skjoldal, H.R., Rey, F., 1990. Predation by copepods upon natural populations of Phaeocystis pouchetii as a function of the physiological state of the prey. Mar. Ecol. Prog. Ser. 67, 235–249.

Falkowski, P.G., Dubinsky, Z., Wyman, K., 1985. Growth-irradiance relationships in phytoplankton. Limnol. Oceanogr. 30, 311–321. https://doi.org/10.4319/lo.1985.30.2.0311.

Frey, K.E., Maslanik, J.A., Kinney, J.C., Maslowski, W., 2014. Recent variability in sea ice cover, age, and thickness in the Pacific Arctic region. In: The Pacific Arctic Region: Ecosystem Status and Trends in a Rapidly Changing Environment. Springer, Netherlands, Dordrecht, pp. 31–63.

Frey, K.E., Moore, G.W.K., Cooper, L.W., Grebmeier, J.M., 2015. Divergent patterns of recent sea ice cover across the bering, chukchi, and beaufort seas of the pacific arctic region. Progress. Oceanogr. 136, 32–49. https://doi.org/10.1016/j.pocean.2015.05.009.

Gosselin, M., Levasseur, M., Wheeler, P.A., Horner, R.A., Booth, B.C., 1997. New measurements of phytoplankton and ice algal production in the Arctic Ocean. Deep-Sea Res. II 44, 1623–1644.

Grebmeier, J.M., 2012. Shifting patterns of life in the pacific arctic and sub-arctic seas. Annu. Rev. Mar. Sci. 4, 63–78. https://doi.org/10.1146/annurev-marine-120710-100926.

Grebmeier, J.M., Bluhm, B.A., Cooper, L.W., Danielson, S.L., Arrigo, K.R., Blanchard, A.L., Clarke, J.T., Day, R.H., Frey, K.E., Gradinger, R.R., Kędra, M., Konar, B., Kuletz, K.J., Lee, S.H., Lovvorn, J.R., Norcross, B.L., Okkonen, S.R., 2015. Ecosystem characteristics and processes facilitating persistent macrobenthic biomass hotspots and associated benthivory in the Pacific Arctic. Progress. Oceanogr. 136, 92–114. https://doi.org/10.1016/j.pocean.2015.05.006.

Grebmeier, J.M., Cooper, L.W., Feder, H.M., Sirenko, B.I., 2006a. Ecosystem dynamics of the Pacific-influenced northern Bering and Chukchi seas in the Amerasian Arctic. Progress. Oceanogr. 71, 331–361.

Grebmeier, J.M., Overland, J., Moore, S.E., Farley, E.V., Carmack, E.C., Cooper, L.W., Frey, K.E., Helle, J.H., McLaughlin, F.A., Lyn McNutt, S., 2006b. A major ecosystem shift in the northern bering sea. Science 311, 1461–1464. https://doi.org/10.1126/science.1121365.

Grebmeier, J.M., Cooper, L.W., Kedra, M., Moore, S., 2018. Time Series Trends in Benthic Macrofaunal Hotspot Sites and Environmental Drivers in the Pacific Arctic. Abstract HE12B-01 presented at 2018 Ocean Sciences Meeting, Portland, OR, 12-16 Feb.

Grebmeier, J.M., McRoy, C.P., 1989. Pelagic-benthic coupling on the shelf of the northern bering and chukchi seas. III. Benthic food supply and carbon cycling. Mar. Ecol. Prog. Ser. 53, 79–91.

Grebmeier, J.M., Moore, S.E., Overland, J.E., Frey, K.E., Gradinger, R., 2010. Biological response to recent Pacific Arctic sea ice retreats. Eos, Trans. 91, 161.

Hama, T., Miyazaki, T., Ogawa, Y., Iwakuma, T., Takahashi, M., Otsuki, A., Ichimura, S., 1983. Measurement of photosynthetic production of a marine phytoplankton population using a stable 13C isotope. Mar. Bio. 73, 31–36.

Hameedi, M.J., 1978. Aspects of water column primary productivity in the Chukchi Sea during summer. Mar. Bio. 48, 37–46.

Hansell, D.A., Goering, J.J., 1990. Pelagic nitrogen flux in the northern Bering Sea. Cont. Shelf Res. 10, 510–519.

Hansell, D.A., Goering, J.J., Walsh, J.J., McRoy, C.P., Coachman, L.K., Whitledge, T.E., 1989. Summer phytoplankton production and transport along the shelf break in the bering sea. Cont. Shelf Res. 9, 1085–1104.

Hansell, D.A., Whitledge, T.E., Goering, J.J., 1993. Patterns of nitrate utilization and new production over the Bering-Chukchi shelf. Cont. Shelf Res. 13, 601–627.

Highsmith, R.C., Coyle, K.O., 1990. High productivity of northern Bering Sea benthic amphipods. Nature 344, 862–864.

Hill, V., Ardyna, M., Lee, S.H., Varela, D.E., 2017. Decadal trends in phytoplankton production in the Pacific Arctic Region from 1950 to 2012. Deep-Sea Res. Ii. https://doi.org/10.1016/j.dsr2.2016.12.015.

Hill, V., Cota, G., 2005. Spatial patterns of primary production on the shelf, slope and basin of the Western Arctic in 2002. Deep-Sea Res. II 52, 3344–3354. https://doi.org/

10.1016/j.dsr2.2005.10.001.

Iida, T., Mizobata, K., Saitoh, S.I., 2012. Interannual variability of coccolithophore Emiliania huxleyi blooms in response to changes in water column stability in the eastern Bering Sea. Cont. Shelf Res. 34, 7–17. https://doi.org/10.1016/j.csr.2011.11.007.

Jeffries, M.O., Overland, J.E., Perovich, D.K., 2013. The Arctic shifts to a new normal. Phys. Today 66, 35–40. https://doi.org/10.1063/PT.3.2147.

Joo, H.M., Lee, S.H., Jung, S.W., Dahms, H.-U., Lee, J.H., 2012. Deep-Sea Research II. Deep-Sea Res. II 81–84, 3–17. https://doi.org/10.1016/j.dsr2.2011.06.004.

Lee, S.H., Joo, H.M., Yun, M.S., Whitledge, T.E., 2012. Recent phytoplankton productivity of the northern Bering Sea during early summer in 2007. Polar Biol. 35, 83–98. https://doi.org/10.1007/s00300-011-1035-9.

Lee, S.H., Whitledge, T., Kang, S., 2007. Recent carbon and nitrogen uptake rates of phytoplankton in Bering Strait and the Chukchi Sea. Cont. Shelf Res. 27, 2231–2249. https://doi.org/10.1016/j.csr.2007.05.009.

Lee, S.H., Yun, M.S., Kim, B.K., Saitoh, S.-I., Kang, C.K., Kang, S.-H., Whitledge, T., 2013a. Latitudinal carbon productivity in the Bering and Chukchi Seas during the summer in 2007. Cont. Shelf Res. 59, 28–36. https://doi.org/10.1016/j.csr.2013.04.004.

Lee, S.H., Yun, M.S., Kim, B.K., Joo, H., Kang, S.-H., Kang, C.K., Whitledge, T.E., 2013b. Contribution of small phytoplankton to total primary production in the Chukchi Sea. Cont. Shelf Res. 68, 43–50. https://doi.org/10.1016/j.csr.2013.08.008.

Li, W.K.W., McLaughlin, F.A., Lovejoy, C., Carmack, E.C., 2009. Smallest Algae Thrive As the Arctic Ocean Freshens (539–539). Science 326. https://doi.org/10.1126/science.1179798.

Lomas, M.W., Glibert, P.M., 1999. Interactions between NH_4^+ and NO_3^- uptake and as-similation: comparison of diatoms and dinoflagellates at several growth tempera-tures. Mar. Bio 133, 541–551.

Lundholm, N., Hasle, G.R., 2010. *Fragilariopsis* (Bacillariophyceae) of the Northern Hemisphere–morphology, taxonomy, phylogeny and distribution, with a description of F. pacifica sp. nov. Phycologia 49, 438–460.

Martin, J., Tremblay, J.É., Price, N.M., 2012. Nutritive and photosynthetic ecology of subsurface chlorophyll maxima in Canadian Arctic waters. Biogeosciences 9, 5353–5371. https://doi.org/10.5194/bg-9-5353-2012.

Mathis, J.T., Grebmeier, J.M., Hansell, D.A., Hopcroft, R.R., Kirchman, D.L., Lee, S.H., Moran, S.B., Bates, N.R., VanLaningham, S., Cross, J.N., Cai, W.-J., 2014. Carbon biogeochemistry of the western arctic: primary production, carbon export and the controls on ocean acidification. In: Grebmeier, J.M., Maslowski, W. (Eds.), The Pacific Arctic Region: Ecosystem Status and Trends in a Rapidly Changing Environment. Springer, Netherlands, Dordrecht, pp. 223–268.

McRoy, C.P., Hansell, D.A., Springer, A.M., Walsh, J.J., Whitledge, T.E., 1987. Global maximum of primary production in the north Bering Sea. Eos, Trans. 68, 172.

Merico, A., Tyrrell, T., Brown, C.W., Groom, S.B., Miller, P.I., 2003. Analysis of satellite imagery for Emiliania huxleyiblooms in the Bering Sea before 1997. Geophys. Res. Lett. 30, 7467. https://doi.org/10.1029/2002GL016648.

Moore, S.E., 2016. Is it "boom times" for baleen whales in the Pacific Arctic region? Biol. Lett. 12, 20160254–20160254. https://doi.org/10.1098/rsbl.2016.0251.

Moore, S.E., Grebmeier, J.M., 2018. The distributed biological observatory: linking physics to biology in the pacific arctic region. Arctic.

Moore, S.E., Stabeno, P.J., 2015. Synthesis of Arctic Research (SOAR) in marine ecosys-tems of the Pacific Arctic. Progress. Oceanogr. 136, 1–11. https://doi.org/10.1016/j.pocean.2015.05.017.

Moore, S.E., Logerwell, E., Eisner, L., Farley, E.V., Harwood, L.A., Kuletz, K., Lovvorn, J., Murphy, J.R., Quakenbush, L.T., 2014. Marine Fishes, Birds and Mammals as Sentinels of Ecosystem Variability and Reorganization in the Pacific Arctic Region. In: Grebmeier, J.M., Maslowski, W. (Eds.), The Pacific Arctic Region. Springer, Netherlands, Dordrecht, pp. 337–392. https://doi.org/10.1007/978-94-017-8863-2_11.

Napp, J.M., Hunt Jr, G.L., 2001. Anomalous conditions in the south-eastern Bering Sea 1997: linkages among climate, weather, ocean, and Biology. Fish. Oceanogr. 10, 61–68.

Nelson, R.J., Ashjian, C.J., Bluhm, B.A., Conlan, K.E., Gradinger, R.R., Grebmeier, J.M., Hill, V.J., Hopcroft, R.R., Hunt, B.P.V., Joo, H.M., Kirchman, D.L., Kosobokova, K.N., Lee, S.H., Li, W.K.W., Lovejoy, C., Poulin, M., Sherr, E., Young, K.V., 2014. Biodiversity and biogeography of the lower trophic taxa of the pacific arctic region: sensitivities to climate change. In: Grebmeier, J.M., Maslowski, W. (Eds.), The Pacific Arctic Region: Ecosystem Status and Trends in a Rapidly Changing Environment. Springer, Netherlands, Dordrecht, pp. 269–336.

Olli, K., Riser, C.W., Wassmann, P., Ratkova, T., Arashkevich, E., Pasternak, A., 2002. Seasonal variation in vertical flux of biogenic matter in the marginal ice zone and the central Barents Sea. J. Mar. Sys. 38, 189–204.

Overland, J.E., Stabeno, P.J., 2004. Is the climate of the Bering Sea warming and affecting the ecosystem? Eos, Trans.

Parsons, T.R., Maita, Y., Lalli, C.M., 1984. A manual of chemical and biological methods for seawater analysis, 1st ed. Pergamon.

Pasciak, W.J., Gavis, J., 1974. Transport limitation of nutrient uptake in phytoplankton. Limnol. Oceanogr. 19, 881–888. https://doi.org/10.4319/lo.1974.19.6.0881.

Platt, T., Harrison, W., Lewis, M., Li, W.K.W., Sathyendranath, S., Smith, R., Vezina, A., 1989. Biological production of the oceans: the case for a consensus. Mar. Ecol. Prog. Ser. 52, 77–88.

Poulin, M., Daugbjerg, N., Gradinger, R., Ilyash, L., Ratkova, T., Quillfeldt, C., 2010. The pan-Arctic biodiversity of marine pelagic and sea-ice unicellular eukaryotes: a first-attempt assessment. Mar. Biodiv 41, 13–28. https://doi.org/10.1007/s12526-010-0058-8.

Sakshaug, E., 2004. Primary and Secondary Production in the Arctic Seas. In: Stein, R., Macdonald, R.W. (Eds.), The Organic Carbon Cycle in the Arctic Ocean, The Organic Carbon Cycle in the Arctic Ocean. Springer, Berlin Heidelberg, Berlin, Heidelberg, pp.

57–81.

Sambrotto, R.N., Goering, J.J., McRoy, C.P., 1984. Large yearly production of phyto-plankton in the western bering strait. Science 225, 1147–1150.

Serreze, M.C., Barrett, A.P., Slater, A.G., Woodgate, R.A., Aagaard, K., Lammers, R.B., Steele, M., Moritz, R., Meredith, M., Lee, C.M., 2006. The large-scale freshwater cycle of the Arctic. J. Geophys. Res. 111, 14485. https://doi.org/10.1029/2005JC003424.

Sherr, E.B., Sherr, B.F., Hartz, A.J., 2009. Microzooplankton grazing impact in the Western Arctic Ocean. Deep-Sea Res. II 56, 1264–1273. https://doi.org/10.1016/j.dsr2.2008.10.036.

Sherr, E.B., Sherr, B.F., Ross, C., 2013. Microzooplankton grazing impact in the Bering Sea during spring sea ice conditions. Deep-Sea Res. II 94, 57–67. https://doi.org/10.1016/j.dsr2.2013.03.019.

Slawyk, G., Collos, Y., Auclair, J., 1977. The Use of the 13C and 15N Isotopes for the simultaneous measurement of carbon and nitrogen turnover rates in marine phyto-plankton. Limnol. Oceanogr. 22, 925–932.

Smith, W.O., Codispoti, L.A., Nelson, D.M., Manley, T., Buskey, E.J., Niebauer, H.J., Cota, G.F., 1991. Importance of phaeocystis blooms in the high-latitude ocean carbon-cycle. Nature 352, 514–516.

Springer, A.M., McRoy, C.P., 1993. The paradox of pelagic food webs in the northern Bering Sea—III. Patterns of primary production. Cont. Shelf Res. 13, 575–599.

Stabeno, P.J., Bond, N.A., Salo, S.A., 2007. On the recent warming of the southeastern Bering Sea shelf. Deep-Sea Res. II 54, 2599–2618. https://doi.org/10.1016/j.dsr2.2007.08.023.

Stabeno, P.J., Danielson, S.L., Kachel, D.G., Kachel, N.B., Mordy, C.W., 2016. Currents and transport on the Eastern Bering Sea shelf: an integration of over 20 years of data. Deep-Sea Res. II 134, 13–29. https://doi.org/10.1016/j.dsr2.2016.05.010.

Steinberg, D.K., Saba, G.K., 2008. Nitrogen consumption and metabolism in marine zooplankton. In: Capone, D., Bronk, D.A., Mulholland, M.R., Carpenter, E.J. (Eds.), Nitrogen in the Marine Environment. Academic Press, pp. 1135–1196.

Stigebrandt, A., 1984. The North Pacific: a global-scale estuary. J. Phys. Oceanogr. 14, 464–470.

Stockwell, D.A., Whitledge, T.E., Zeeman, S.I., Coyle, K.O., Napp, J.M., Brodeur, R.D., Pinchuk, A.I., Hunt Jr, G.L., 2001. Anomalous conditions in the south-eastern Bering Sea, 1997: nutrients, phytoplankton and zooplankton. Fish. Oceanogr. 10, 99–116.

Stroeve, J.C., Markus, T., Boisvert, L., Miller, J., Barrett, A., 2014. Changes in Arctic melt season and implications for sea ice loss. Geophys. Res. Lett. 41, 1216–1225.

Sukhanova, I.N., Flint, M.V., Pautova, L.A., Stockwell, D.A., Grebmeier, J.M., Sergeeva, V.M., 2009. Phytoplankton of the western Arctic in the spring and summer of 2002: structure and seasonal changes. Deep-Sea Res. II 56, 1223–1236. https://doi.org/10.1016/j.dsr2.2008.12.030.

Utermohl, H., 1958. Zur Vervollkommnung der quantitativen Phytoplankton-Methodik. Internationale Vereinigung für Theoretische und Angewandte Limnologie. Kom. für Limnol. Methode. 9, 1–39.

Varela, D.E., Harrison, P.J., 1999. Effect of ammonium on nitrate utilization by Emiliania huxleyi, a coccolithophore from the oceanic northeastern Pacific. Mar. Ecol. Prog. Ser. 186, 67–74.

Varela, D.E., Crawford, D.W., Wrohan, I.A., Wyatt, S.N., Carmack, E.C., 2013. Pelagic primary productivity and upper ocean nutrient dynamics across Subarctic and Arctic Seas. J. Geophys. Res. Oceans 118, 7132–7152. https://doi.org/10.1002/2013JC009211.

Walsh, J.J., McRoy, C.P., Coachman, L.K., Goering, J.J., Nihoul, J.J., Whitledge, T.E., Blackburn, T.H., Parker, P.L., Wirick, C.D., Shuert, P.G., 1989. Carbon and nitrogen cycling within the Bering/Chukchi Seas: source regions for organic matter effecting AOU demands of the Arctic Ocean. Progress. Oceanogr. 22, 277–359.

Wassmann, P., Duarte, C.M., Agustí, S., Sejr, M.K., 2010. Footprints of climate change in the Arctic marine ecosystem. Glob. Change Biol. 17, 1235–1249. https://doi.org/10.1111/j.1365-2486.2010.02311.x.

Wassmann, P., Ratkova, T., Andreassen, I., Vernet, M., Pedersen, G., Rey, F., 1999. Spring bloom development in the marginal ice zone and the central Barents Sea. Mar. Ecol. 20, 321–346.

Weingartner, T.J., Danielson, S., Sasaki, Y., Pavlov, V., Kulakov, M., 1999. The Siberian Coastal Current: a wind- and buoyancy-forced Arctic coastal current. J. Geophys. Res. 104, 29697–29713.

Wood, K.R., Bond, N.A., Danielson, S.L., Overland, J.E., Salo, S.A., Stabeno, P., Whitefield, J., 2015. A decade of environmental change in the Pacific Arctic region. Progress. Oceanogr. 136, 12–31. https://doi.org/10.1016/j.pocean.2015.05.005.

Woodgate, R.A., 2018. Increases in the Pacific inflow to the Arctic from 1990 to 2015, and insights into seasonal trends and driving mechanisms from year-round Bering Strait mooring data. Progress. Oceanogr. 160, 124–154. https://doi.org/10.1016/j.pocean.2017.12.007.

Woodgate, R.A., Aagaard, K., Weingartner, T.J., 2005a. A year in the physical oceano-graphy of the Chukchi Sea: moored measurements from autumn 1990–1991. Deep-Sea Res. II 52, 3116–3149. https://doi.org/10.1016/j.dsr2.2005.10.016.

Woodgate, R.A., Aagaard, K., Weingartner, T.J., 2005b. Monthly temperature, salinity, and transport variability of the Bering Strait through flow. Geophys. Res. Lett. 32. https://doi.org/10.1029/2004GL021880.

Woodgate, R.A., Weingartner, T., Lindsay, R., 2010. The 2007 Bering Strait oceanic heat flux and anomalous Arctic sea-ice retreat. Geophys. Res. Lett. 37. https://doi.org/10.1029/2009GL041621.

Woodgate, R.A., Weingartner, T.J., Lindsay, R., 2012. Observed increases in Bering Strait oceanic fluxes from the Pacific to the Arctic from 2001 to 2011 and their impacts on the Arctic Ocean water column. Geophys. Res. Lett. 39. https://doi.org/10.1029/2009GL041621.

Wyatt, S.N., Crawford, D.W., Wrohan, I.A., Varela, D.E., 2013. Distribution and compo-sition of suspended biogenic particles in surface waters across Subarctic and Arctic Seas. J. Geophys. Res. Oceans 118, 6867–6880. https://doi.org/10.1002/

2013JC009214.

Yamamoto-Kawai, M., Carmack, E., McLaughlin, F., 2006. Nitrogen balance and Arctic throughflow (43–43). Nature 443. https://doi.org/10.1038/443043a.

Yun, M.S., Whitledge, T.E., Kong, M., Lee, S.H., 2014. Low primary production in the Chukchi Sea shelf, 2009. Cont. Shelf Res. 76, 1–11. https://doi.org/10.1016/j.csr.2014.01.001.

Żurek, R., Bucka, H., 1994. Algal size classes and phytoplankton-zooplankton interacting effects. J. Plankton Res. 16, 583–601.

Further reading

Tozzi, S., Schofield, O., Falkowski, P.G., 2004. Historical climate change and ocean turbulence as selective agents for two key phytoplankton functional groups. Mar. Ecol. Prog. Ser. 274, 123–132.

Woodgate, R.A., Aagaard, K., 2005. Revising the Bering Strait freshwater flux into the Arctic Ocean. Geophys. Res. Lett. 32 (14), 485. https://doi.org/10.1029/2004GL021747.